Impact of natural (waves and currents) and anthropogenic (trawl) resuspension on the export of particulate matter to the open ocean. Application to the Gulf of Lion (NW Mediterranean)

B. Ferré[1], X. Durrieu de Madron[1], C. Estournel[2], C. Ulses[2], G. Le Corre[3]

[1]CEFREM, CNRS-Université de Perpignan, Perpignan France

[2]LA, CNRS-Université Paul Sabatier, Toulouse France

[3]IFREMER, DRH, Sète France

ABSTRACT

Modern sediment deposits on continental margins form a vast reservoir of particulate matter that is regularly affected by resuspension processes. Resuspension by bottom trawling on shelves with strong fishing activity can modify the scale of natural disturbance by waves and currents. Recent field data show that the impact of bottom trawls on fine sediments resuspension per unit surface is comparable with that of the largest storms.

We assessed the impact of both natural and anthropogenic processes on the dispersal of river-borne particles and shelf sediments on the Gulf of Lion shelf. We performed realistic numerical simulations of resuspension and transport forced by currents and waves or by a fleet of bottom trawlers. Simulations were conducted for a 16-month period (January 1998 - April 1999) to characterise the seasonal variability. The sediment dynamics takes into account bed armoring, ripple geometry and the cohesive and non-cohesive characteristics of the sediments. Essential but uncertain parameters (clay content, erosion fluxes and critical shear stress for cohesive sediment) were set with existing data. Resuspension by waves and currents was controlled by shear stress, whereas resuspension by trawls was controlled by density and distribution of the bottom trawler fleet.

Natural resuspension by waves and currents mostly occurred during short seasonal episodes, and was concentrated on the inner-shelf. Trawling-induced resuspension, in contrast, occurred regularly throughout the year and was concentrated on the outer shelf. The total annual erosion by trawls (5.6×10^6 t y^{-1}, t for metric tonnes) was four orders of magnitude lower than the erosion induced by waves and currents (35.3×10^9 t y^{-1}). However the net resuspension (erosion/deposition budget) for trawling (0.4×10^6 t y^{-1}) was only one order of magnitude lower than that for waves and currents (9.2×10^6 t y^{-1}).

Off-shelf export concerned the finest fraction of the sediment (clays and fine silts) and took place primarily at the southwestern end of the Gulf. Off-shelf transport was favoured during the winter 1999 by a very intense episode of dense shelf water cascading. Export of sediment resuspended by trawls (0.4×10^6 t y^{-1}) was one order of magnitude lower than export associated with natural resuspension (8.5×10^6 t y^{-1}). Trawling-induced resuspension is thought to represent one third of the total export of suspended sediment from the shelf.

A simulation combining both resuspension processes reveals no significant changes in resuspension and export rates compared with the sum of each individual process, suggesting the absence of interference between both processes.

Keywords: Sediment dynamics; Sediment transport; Shelf–slope exchanges; Fisheries; Trawling; Mediterranean

1. INTRODUCTION

Continental margins are located at the edges of continents and form a buffer zone where the oceans, continents and atmosphere interact. Significant quantities of organic and inorganic material are input to continental margins where intense hydrodynamic conditions control their dispersal on the shelf and towards the open sea. The sedimentary compartment on continental margins appears to be a vast reservoir of particulate matter, in particular river-derived material, and also of dissolved constituents. Resuspension of sediment causes a significant redistribution of sediments and has important implication for regional particulate matter budgets and export to deeper environments, i.e. the continental slope and rise.

Nowadays the physical resuspension and disturbance of sediment on continental shelves is a combination of both natural and anthropogenic mechanisms. Waves and currents are the major initiators of natural disturbance that can result in potentially massive sediment redistribution. The large-scale disturbance they induce can be periodic, when associated with tidal currents, or episodic, when associated with storms. On the other hand, commercial bottom trawling has a more reduced and patchy print. Bottom fishing gears (trawl, dredge) efficiently scrape the superficial sediment and generate suspended sediment plumes. In many shelves fishing intensity is high and most fishable grounds, which can extend to 1000 m in depth, are likely to be disturbed more or less frequently. The effect of sediment resuspension by waves and currents and bottom trawling is site-specific, as it depends on hydrodynamic conditions (storm frequency and intensity, tidal motions), sediment characteristics (grain size, cohesiveness), and fishing activity (frequency and geographical distribution of bottom hauls, gear type).

The relative contribution of each mechanism to the resuspension and export of sediment on continental shelves has seldom been addressed. To our knowledge, Churchill (1989) and DeAlteris *et al.* (1999) carried out the only preliminary studies on the comparison of the effect of natural and anthropogenic resuspension on different areas of the Mid-Atlantic Bight (Narraganset Bay, Nantucket Shoals, and Virginia Shelf). These studies concluded that natural physical processes are the primary suspension mechanism in shallow environments, where they disturb the bed regularly, while trawling appears to be the primary resuspension mechanism in deeper environments where natural processes are weaker and rarely capable of eroding sediment. Furthermore, Churchill (1989) estimated, using current meter data and simple analytical models, that transport of sediment resuspended by trawlers on muddy regions of the outer shelf could contribute to the off-shelf transport of particulate matter.

The present paper aims to assess the impact of sediment resuspension on particulate matter budgets on the Gulf of Lion continental shelf (NW Mediterranean). It discriminates the impact of natural physical (waves and currents) and anthropogenic (bottom trawling) processes, and thereby evaluates whether anthropogenic disturbance represents a significant or just a slight modification in the scale of

existing natural disturbance. This work uses three-dimensional numerical models coupling the hydrodynamics with the sediment dynamics associated with waves and currents and/or trawling. The parameterizations used in the models are based on experimental studies of the resuspension of fine sediments by intense storms (Ferré *et al.*, 2005; Ulses *et al.*, this volume) and trawls (Durrieu de Madron *et al.*, 2005). Simulations over one annual period, using realistic forcings, were carried out to characterise and quantify (i) the temporal variability and magnitude of sediment resuspension on the shelf, (ii) the dispersal of resuspended sediment, and (iii) the export towards the open sea.

The outline of this paper is as follows: the regional setting is described in section 2, the hydrodynamical and sediment transport models are briefly described in section 3, the numerical simulations of sediment resuspension and export are exposed in section 4, comparison of resuspension processes and their impact of the sediment budgets are presented in section 5, a summary is given in section 6, and the model equations are given in the appendix.

2. REGIONAL SETTING

2.1. Physiography and hydrodynamics

The Gulf of Lion is a non-tidal and river-dominated margin in the northwestern Mediterranean (Fig. 1a). It is fed by ten rivers, one of them being the Rhône, which is the major Mediterranean river. Its crescent shape and the circulation patterns favour off-shelf export of particulate matter at the southwestern end of the Gulf (Monaco *et al.*, 1999; Heussner *et al.*, 2006, Palanques *et al.*, 2006).

The grain size distribution of superficial bottom sediments is shown in Fig. 1b. Sands of the inner shelf display a seaward-fining texture and merge with mid-shelf muds in water deeper than 20–30 m. The only noticeable exception is the prodeltaic accumulation zones found near river mouths, which are composed of silty muds. Muddy deposits on the outer shelf (>90 m) are mixed with relict sandy outcrops.

The different wind regimes determine the natural resuspension and transport of suspended sediment on the shelf. Predominant N-NW winds generally induce distinctive and opposing circulation cells on the shelf, favouring intrusion of slope waters in the eastern and central parts, and export of shelf water at the southwestern end of the Gulf (Estournel *et al.*, 2003; Petrenko *et al.*, 2004, Ulses et al., in press)). Furthermore, these cold and dry continental winds are responsible for the strong cooling and homogenisation of the shelf water column during winter, and eventually generate dense water (Dufau-Julliand *et al.*, 2004; Ulses *et al.*, in press). Due to the reduced fetch, N-NW winds generate small waves (significant wave height < 2 m, peak period < 6 s) on the inner shelf. Episodic and short-lived E-SE winds induce a sea level rise at the shore and an overall intense cyclonic circulation on the shelf (Ulses *et al.*, in press). These winds are, are associated with a long fetch and large swell

(significant wave height up to 10 m, peak period up to 12 s). River floods often occur in conjunction with E-SE storms as the transport of humid marine air over coastal relief induces abundant precipitation. Resuspension by natural physical processes results primarily from the effect of southeasterly swells associated with E-SE winds (Ferré *et al.*, 2005, Guillén *et al.*, 2006).

A permanent cyclonic current (the Northern Current) flows along the slope and is part of the general circulation of the western Mediterranean basin (Millot, 1999). It forms a density front that separates the low-salinity shelf water from the more saline open sea water, limiting the off-shelf dispersal while enhancing along-slope dispersal (Durrieu de Madron *et al.*, 1990; Lapouyade and Durrieu de Madron, 2001).

Hence, constrained by the slope current offshore and the coast inshore, most shelf water and suspended sediments are funneled towards the narrowing southwestern shelf end. They are advected out of Gulf of Lion's shelf, by flowing alongshore around the Cape Creus promontory or down the nearby canyons.

2.2. Characteristics of trawling activity

About 128 trawlers coming from the local fishing ports (Port-Vendres, Port-la-Nouvelle, Agde, Sète, Grau du Roi, Port de Bouc) are working in the Gulf of Lion, using either semi-pelagic or bottom trawls to catch demersal fish species. Bottom trawlers use single trawl nets tightened between doors (otter) with a tickler chain as a groundrope. Pelagic trawls are sometimes also used very near the seabed, but Durrieu de Madron *et al.* (2005) showed that they had no impact on the sediment resuspension. The daily number of trawlers using bottom trawls ranges approximately between 40 and 90 boats, each trawler performing 4 to 5 tows of about 2 hours daily. They work throughout the year except weekends and public holidays.

Fishing grounds cover the whole continental shelf except for a 3-mile coastal band, where all trawling activity is banned. A survey conducted with fishermen revealed that the wind is the principal criterion for the choice of the fishing grounds. Trawlers remain basically close to the coast during strong winds (> 10 m s^{-1} or 20 knots) and rough seas state periods, and move to the outer shelf for weaker winds and calmer sea state..

3. MATERIAL AND METHODS

3.1. Hydrodynamical model

The SYMPHONIE Model - The three-dimensional primitive equation coastal ocean model SYMPHONIE, used in this study, has been extensively validated in the Gulf of Lion. It was previously used to study the Rhône river plume (Estournel *et al.*, 1997; Marsaleix *et al.*, 1998; Estournel *et al.*, 2001), the intrusion of the Northern Current into the shelf (Petrenko *et al.*, 2004), the wind-induced circulation (Estournel *et al.*, 2003) and the formation of dense water on the shelf and its cascading over the slope (Dufau-Julliand *et al.*, 2004; *Ulses et al.*, accepted).

The horizontal and verticalcomponents of the current, free surface elevation, temperature and salinity are computed on a C staggered-grid (Arakawa and Suarez, 1983). A generalized topography following co-ordinate system is used. Compared to simple sigma coordinate, the generalized sigma coordinate allows the slope of the iso-level surface to be limited over steep topography in order to avoid large truncation errors on the pressure gradient computation (Auclair *et al.*, 2000). The turbulence closure scheme is based on a prognostic equation for the turbulent kinetic energy and on a diagnostic equation for the mixing and dissipation length scales (Bougeault and Lacarrère, 1989). A leap frog scheme is used for the time-stepping. A time-splitting technique (Blumberg and Mellor, 1987) allows the vertical shear of the current and the depth-averaged horizontal components to be computed separately with appropriate time steps. The time step of the model is set to 180 s.

Initialisation and boundary conditions - The domain of the Gulf of Lion model (25 vertical levels and 3 km horizontal resolution grid) is presented in Figure 1a. The main boundary of the modelling domain has been chosen to be parallel to the continental slope.

At the surface, the momentum flux is equal to the wind stress. The heat flux results from the atmospheric fluxes (sensible and latent heat fluxes) and from the radiative fluxes (both short and long wavelengths), the salinity flux is calculated from evaporation. Concerning the flux of turbulent kinetic energy, the usual boundary-layer balance between production and dissipation is applied. The wind stress and the heat fluxes are computed with the bulk formulae (Geernaert, 1990) using 6-hours outputs of the high resolution meteorological models ARPEGE and ALADIN from Météo-France (surface pressure, air temperature, relative humidity and wind velocity) and the sea surface temperature is computed by the ocean model.

At the sea floor, the near-bottom stress is related to the horizontal bottom velocity and waves, as well as the seabed roughness. A detailed description of this term is given in appendix 2. Heat and salinity fluxes are considered to be zero at this boundary. The flux of turbulent kinetic energy is parameterised similarly as the one at the surface boundary.

At open lateral boundaries, the free-surface elevation (η) and the component of transport orthogonal to the boundary (U) are given by the radiation condition of Oey and Chen (1992): $U=U_0 \pm (gH)^{1/2} (\eta-\eta_0)$. Others variables are given by $\nabla_H\varphi = \nabla_H\varphi_0$, where φ stands for the tangential component of the depth

averaged current and baroclinic velocities. U_0, φ_0 and η_0 refer to the large scale field forcing. Concerning temperature and salinity, an upstream condition implies that large-scale fields, T_0 (t) and S_0 (t), are advected into the simulated domain under inflow conditions. The large-scale fields are also applied over the whole grid at $t=t_0$ (initialisation). This initial state aims to start the simulation with the large-scale geostrophic circulation of the Gulf of Lion, generally identified as the Northern Current. The model is initialised with a fully established along slope circulation adjusted to bathymetry constraints, based on a linearised derivation of the external mode equations of the model (Estournel *et al.*, 2003). The regional model was initialized and forced every day by the large scale Ocean General Circulation Model (OGCM) MOM outputs. Wave characteristics over the domain were described by the 6-hour outputs of the Vagmed waves-forecast model of Météo-France.

Concerning the buoyancy inputs, the freshwater inputs for the main rivers of the Gulf of Lion (Grand-Rhone, Petit-Rhone, Vidourle, Lez, Herault, Orb, Aude, Agly, Têt, Tech) (see Fig. 1a), are taken into account. Daily discharges provided by the 'Compagnie Nationale du Rhône' and by the 'Banque Hydro-MEDD/DE' were specified at the ten river mouths. The temperature in all rivers is set following measurements in Rhone river (Poirel *et al.*, 2001), with a maximum value of 22 °C in October and a minimum value of 7 °C in January and February.

3.2. Sediment transport model

The suspended sediment transport model aims at simulating the dispersal of the sedimentary particles resuspended by waves and currents, as well as bottom trawls. This model is governed by an advection-diffusion dispersion equation, and considers different particle grain sizes (see appendix 1). Deposition and erosion terms are incorporated into the seabed boundary condition. The erosion term was estimated with sediment dynamic models specific to each resuspension mechanisms (waves and current, trawl); they are described in the following chapters and in appendix 2.

Given that the Gulf of Lion sediments cover a wide range of size (Fig. 1b), primary (individual) particles in the sediment were clustered in 7 size classes ranging from clay to coarse sand, according to the Wentworth classification (1922). Two additional classes were considered for suspended particles to take into account aggregated particles. The aggregates characteristics were inferred from comparisons between *in situ* and laboratory particle size distribution of resuspended sediment (Durrieu de Madron *et al.*, 2005). These measurements suggested that about ¾ of the clays and ¼ of the fine silts are incorporated into aggregates whereas the rest remains as primary particles. We considered that clays and fine silts contributed equally to the formation of both classes of aggregates. The characteristics of each class (median grain size, settling velocity and density) are indicated in the Table 1.

River sediment inputs were computed using water discharge (Q) and suspended sediment concentration estimates (SSC=f(Q)) established by different authors: Sempéré *et al.* (2000) for the Rhône River, Petelet-Giraud *et al.* (2003) for the Herault River, Serrat (1999) for the Agly River, and

Serrat *et al.* (2001) for the Têt River. In absence of information for Orb and Aude Rivers, we used the relationship of the nearby Herault River. Finally, solid discharge of the Rhône River was divided into two parts: 90% for the Grand-Rhône branch and 10% for the Petit-Rhône branch. Grain size distribution of river inputs was defined according to recent data collected in the Rhône River (Radakovitch, personal communication) and Têt River (Garcia-Esteves, 2005). All "small" rivers (Hérault, Agly, Orb, Aude, Vidourle and Tech) are considered to have the same grain distribution as the Têt River. Most of the suspended particles are silts (ca 80% for the Rhône River and 69% for the Têt River) and clays (~ 18% for the Rhône River and 24% for the Têt River). The sediment provided by the rivers is homogeneously input in one mesh, and settles and/or is transported as it enters the domain.

The grain size distribution of the shelf surface sediments was determined from the compilation of several sedimentological surveys that provided about 160 cores over the whole shelf. Figure 1b shows the median grain size of the first centimetres of the sediment. Maps of the fraction of the different size classes were used at the initial time. Their characteristics slightly changed throughout the simulation according to the dispersal of river inputs, and the erosion and deposition of the different classes of sediment.

3.3. Sediment dynamics for waves and currents

The sediment erodability is controlled by the shear stress intensity and the bottom sediment properties (coarse non-cohesive vs. fine cohesive sediments). The limit between cohesive and non-cohesive sediment was fixed at 10 % of clay (<2 µm), which is in the range (3-14%) defined in various studies (Dyer, 1986; Torfs, 1995; Panagiopoulos *et al.*, 1997; Houwing, 2000). The Partheniades' law (1962) was used to compute the erosion flux of cohesive sediments, whereas the reference concentration based on the method of Zyserman and Fredsøe (1994) was used for the erosion flux of the non-cohesive sediments (see appendix 2).

The stress values were computed using combined wave and currents conditions, and discriminated flat-bed and rippled bed conditions (see appendix 2). The bottom roughness calculation and ripple geometry for the non-cohesive sediments were based on the SEDTRANS96 model (Li and Amos, 1998; Li and Amos, 2001), which predicts the roughness and bedforms generated by a combined wave/current model. For cohesive and mixed sediments, the roughness scale model of Harris and Wiberg (2001) was used. Besides, bed armoring was implemented in the model to take into account the reduction of erosion flux of fine particles in mixed sediments, due to the protective effect of larger sand grains (Harris and Wiberg, 2001).

The critical shear stress (stress above which the sediment is likely to be removed) depends on grain size and sediment characteristics. For non-cohesive sediments, the critical shear stress is given in the form of a critical Shields parameter value, which depends on the grain size of each class (see appendix 2). For cohesive sediments, the threshold value is difficult to establish because it depends on the compaction and history of the sediment. Indeed, an unconsolidated surface layer (fluff) is

eroded for very weak shear stresses, ranging between 0.02 and 0.08 N m^2 (El Ganaoui *et al.*, 2004; Gust and Morris, 1989; Maa *et al.*, 1998; Schaaff *et al.*, 2002). The underlying, more consolidated layers, need larger critical shear stresses, between 0.1 and 0.61 N m^2 (Maa *et al.*, 1998; Houwing, 1999; Krishnappan and Marsalek, 2002, Palanques *et al.*, 2002). In this study the model does not include a fluff layer, and all of the cohesive sediment is given an average critical shear stress of 0.2 N m^{-2}.

3.4. Resuspension by bottom trawls

In absence of direct information of distribution and movement of trawlers on the shelf (such as those provided by Vessel Monitoring System), we used a probabilistic approach and the fishing rules in force in the area to simulate their daily position and trajectory. Based on sample surveys of the fishermen population of the different ports about their preferential fishing grounds and depths, we derived an average trawling activity within a daily operating range from each port. These fishing patterns were generalized to the trawling fleet of each port, and the total fishing intensity in every locations of the shelf was derived by summing the effect of all fleets. The scores assigned to each location of the shelf area were finally used to weight partition the total fishing effort (Fig. 2). A distribution of fishing effort was simulated for wind speeds lower and larger than 10 m s^{-1}; the sea state being determinant for the choice of fishing grounds. The daily working time and number of active bottom trawlers was estimated from records of trawler fleet coming from the different fishing ports (Fig. 3d). During working days (i.e., apart from weekends and public holidays), each trawler was assumed to perform 4 tows of 2 hours from 4 a.m. to 12 a.m.

The distribution map for each working day was selected according to the wind intensity next to the Sète port (major fishing port of the area) at 4 a.m. After being positioned randomly, each trawl was displaced using a random walk approach. Given the mesh size of the model (3 km) and the trawling speed (1.5 m s^{-1}), a crossing time of 33 min was considered before moving each trawler to one of the surrounding mesh. After this time, the 8 surrounding cells have the same probability to be trawled. A maximum number of 3 trawlers per mesh was imposed, to take into account interaction among fishing vessels. Albeit schematic, the simulated spatial allocations is believed to correctly reproduced the distribution of bottom trawling effort and displacement of vessels, but probably under estimate trawling activity in banned areas (e.g., within the 3-miles coastal band).

The fluxes of sediment resuspended by otter bottom trawls and the characteristics of the sediment plumes were estimated experimentally and described by Durrieu de Madron *et al.* (2005). They showed that resuspension fluxes depend on the trawls groundrope gears, but above all, on sediment texture,i.e., fluxes increase with increasing clay content. Based on the measurements performed by Durrieu de Madron et al. (2005), a linear relationship was derived between the resuspension flux and the clay fraction (see appendix 2). According to observations, resuspended sediment was distributed over the last 5 m above the seabed with a concentration inversely proportional to the seabed distance.

For each time step (180 s), the resuspended mass of sediment in the model is calculated according to the clay fraction and is proportional to the trawled area: 4320 m^2 considering a trawler speed of 1.5 m s^{-1}, and a combined net and door width of 16 m. Because this area is much smaller than that of the model's mesh (9 km^2), the resuspended mass was spread over the entire mesh and within layers including the last 5 m above bottom. The bias introduced by the forced diffusion is likely to be small, since most of the resuspended sediment is rapidly deposited (within 1-2 hours according to Durrieu de Madron *et al.*, 2005), and remains confined to the adjacent meshes.

3.5. Scenarios and numerical solutions

Four scenarios were carried out in order to answer the question about the role of resuspension in the shelf-slope exchanges of particulate matter. They considered the same hydrodynamic forcings described in chapter 3.1.

- The first simulation, which only takes into account the river particulate inputs, (i.e. resuspension is absent), was used as reference for the shelf deposit and the export of riverine particulate matter for the study period;

- The second scenario considered, in addition to the preceding simulation, resuspension of sediment by currents and waves only;

- The third scenario considered the sediment resuspension by trawls only;

- A fourth scenario combining resuspension by waves and currents, as well as trawls, checked if there is any significant non linear effect.

Simulations lasted 16 months from January 1, 1998 to April 1, 1999. The water column was clear of suspended particles at the initial time, and the system was gradually loaded in suspended particles, coming from rivers and/or sediment resuspension during the first months of simulations. As the residence time of shelf waters is about 2 months (Durrieu de Madron *et al.*, 2003), we checked that the suspended sediment concentration (SSC) of the shelf water was stabilized on the third month (March 1998). For each scenario, annual budgets of resuspended sediment, deposited particles on the shelf, and exported particles to the slope, were calculated between April 1998 and April 1999. The shelf-edge for these calculations is defined as the 200-m isobaths, and confined between Cape Creus and Cape Couronne (cf. Fig. 1a for the boundary). Sediment export from the Gulf of Lion's shelf is calculated by the difference between the resuspension and the deposition on the shelf and at each time step, and then by subtracting the sediment present in the water column.

Hydrology and circulation on the shelf and upper slope were measured for two surveys conducted in March/April 1998 and January 1999. Previous studies tested the ability of the hydrodynamical model to correctly reproduce the hydrology and the wind-induced circulation patterns observed in March/April 1998 (Estournel *et al.*, 2003), and the formation of dense water on the shelf and its cascading over the

slope in January/February 1999 (Dufau-Julliand *et al.*, 2004). Critical but indefinite parameters of the sediment dynamics model (i.e., clay content threshold for cohesive/non-cohesive behaviour, erosion flux and critical shear stress for cohesive sediments) were adjusted to fit the *in situ* observations collected all over the shelf during these surveys. Parameters were chosen in order to have the smallest relative error ($| SSC_{in\ situ} - SSC_{model} | / SSC_{in\ situ}$), keeping in mind that measured concentrations include other sources of particulate matter (atmosphere, rivers, biology or advection onto the domain) which are not taken into account in the model. For these reasons, stations nearby the Rhône river mouth, nearby the slope or outside of the shelf are not used because they are likely to contain a majority of particles which are not from resuspension. The location of the casts used for comparison is shown in Fig. 1a. The agreement was quantified by computing the relative error between simulated SSC values (combining both resuspension by waves and current conditions and trawling activity) within the last three levels above the bottom with observed near-bottom SSC, estimated from optical (light transmission) measurements. This comparison is possible because of a weak fluorescence during the surveys (< 0.2 on the Gulf of Lion), indicating a negligible biological fraction. Extreme parameters from the literature were first tested and the adjusted parameters yielded a relative error in SSC less than 35% for more than half of the stations and maximum differences of 80%**.**

4. RESULTS

4.1. Hydrodynamical conditions.

During the simulation period (April 1998 – April 1999) the Rhône River supplied respectively 80% of the freshwater and 90% of the suspended sediment inputs to the Gulf (Fig. 3a). The annual total solid discharges amounted to 3.6×10^6 t (metric tonnes), that were supplied during medium floods occurring mostly during the spring 1998 and late autumn 1998-winter 1999 (Fig. 3b). Given that the average sediment discharge from the Rhône over the 1977-2004 period is about 10.1×10^6 t y^{-1} and peaks at more than 33×10^6 t y^{-1} (Bourrin *et al.*, 2007), the 1998-1999 period appears as a low discharge year.

E-SE gales were rare and brief but caused locally strong precipitations and sudden floods. N-NE continental winds were predominant throughout the year (Fig. 3c). These cold and dry winds affected the annual cycle of the shelf water thermal characteristics, by inducing strong mixing and cooling during fall and winter. As the average salinity of the shelf water was rather constant all over the year, decreasing temperature induced a progressive increase of density that culminated in late winter (Fig. 3f). During winter 1999, dense shelf water overflowed the shelf break and cascaded down the slope . Export of water mainly occurred in the western part of the shelf, and was compensated by an inflow in the eastern part of the Gulf (Fig. 3g). Béthoux *et al.* (2002) showed that an event of such intensity had not occurred since 1993, and that the last event probably went back to the winters 1987-1988. An event of similar intensity was observed in winter 2005 (Canals *et al.*, 2006).

Bottom stress presents a seasonal cycle with larger values between the end of autumn and the beginning of spring (Fig. 3e), due to the increase of the current intensity and wave conditions, and also to the weak stratification or even vertical homogeneity of the shelf water. Wind intensity and direction variability induced many bursts in the bottom stress, which was generally more intense on the western part of the shelf.

In summary, the study period was characterized by low river discharges and moderate wave conditions (with few E-SE storms), but by intense winter shelf water export through dense water cascading caused by sustained N-NW winds.

4.2. Fate of river inputs without resuspension.

A first simulation was carried out by taking into account the sediment supplied by rivers only, in order to estimate the direct contribution of rivers to the sediment export (Fig. 4). During the April 1998 - April 1999 period 3.6×10^6 t of sediment were discharge by rivers (Table 2). As previously mentioned, most input derived from the Rhône River. Deposits of river sediment on the shelf, which amount to 3.1×10^6 t, clearly reflect the difference in river discharges (Fig. 3a). Sediments supplied by the Hérault, Orb, and Aude Rivers in the northwestern part of the Gulf remained primarily confined to the inner shelf. Deposit of the Rhône River inputs formed a wedge extending over the eastern part of the shelf and the outer shelf as far as the southwestern end of the Gulf. The net deposit thickness was largest near the major river mouth, and was about 0.1 mm on most of the shelf. The grain size distribution reflected the accumulation gradient, with an early settling of the coarser particles on the prodeltas, and a fining texture along the transport pathways. Sediments in suspension exported from the shelf were mainly composed of fine particles. The exported quantity was 0.4×10^6 t (only 11% of river inputs (Table 2 and Fig. 5) and two thirds of the export occurred during the wintertime (Dec. 1998 – Apr. 1999).

4.3. Dynamics of resuspended sediments

Resuspension and off-shelf sediment export induced by waves and currents – Time series of the daily mass of sediment resuspended on the shelf (Fig. 6a) showed that resuspension by waves and currents appeared as short events, with a maximum duration of a few days, throughout the year. Some larger and longer resuspension events were noted in spring and fall 1998, and also during December 1998 and February 1999, due to the action of stronger coastal currents or swells. During the April 1998 - April 1999 period about 35.3×10^9 t of sediment were resuspended (Table 2), preferentially on the inner shelf (water depth < 50 m (Fig. 7), and the largest part was composed of

coarse sediments that quickly settled. The annual net erosion/deposition budget amounted to 9.2×10^6 t (Table 2), which was more than twice the annual river inputs.

Off-shelf export occurred as bursts, which immediately followed the resuspension events. They were generally of short duration except for a sustained period in February and March 1999 due to dense shelf water cascading (Fig. 6b). Water flux at the shelf break (Fig. 3g) indicated that the two summer pulses on mid-June and mid-September 1998 occurred on the eastern part of the Gulf, while all the other episodes occurred in its western part. The annual export of sediment solely resuspended by waves and currents amounted to 8.5×10^6 t (Fig. 5), which represented about 0.02% of the resuspended quantity (Table 2). The exported sediment was mostly composed of clays and fine silts, but the strong cascading-driven currents induced an export of larger particles (including sands) during the winter 1999.

The map of erosion and deposition regions at the end of the annual cycle (Fig. 7) indicated a net deposit over most of the shelf, except within the coastal band shallower than 30 m, and also on the southwestern outer shelf. Resuspension by waves and currents induced a total redistribution of the riverine sediments, but did not significantly change the initial grain size distribution of the shelf sediments (i.e., cross-shelf gradient with coarser sediment near the coast and finer sediment seaward). Regions of stronger deposit were localised along a band between 30 and 70 m deep, extending from the Rhône River as far as Cape Creus, which constitutes a natural outlet at the southwestern end of the Gulf. This band, which mimics the mid-shelf mud belt, was primarily composed of fine particles. Distinct patches of deep erosion of sediment by waves and currents were confined to the western gulf and extended to the 500 m isobath. This erosion occurred mainly during the winter cascading period and are related to the convergence and acceleration of dense bottom flow toward the southern end of the shelf and down the head of the canyons.

The dispersal of suspended sediment on the slope was variable according to the period of the year. From May to November, while the water column was stratified, the export of shelf suspended sediment was primarily restricted to the surface slope waters (Fig. 8a). The seaward dispersal in the upper layer (0-500m) was limited by the core of the permanent cyclonic Northern Current that sweptthe material escaping from the shelf along the slope,. From December to April, whilst the water column was weakly stratified or even unstable during the dense water cascading period, shelf suspended sediment rapidly spread into intermediate (500-1000 m) or deep (> 1000 m) slope waters (Fig. 8b).

Resuspension and off-shelf sediment export induced by trawls - In contrast to the natural resuspension which occurs as irregular and short episodes, bottom trawling activity is periodic and rather constant over the whole year (Fig. 3d). Resuspension by trawls is dependant on the trawl number and positions. During the April 1998 - April 1999 period, bottom trawlers worked 250 days and the fishing fleet had a daily mean strength of 63 boats. The total surface scraped by trawlers during this annual period amounted to 11,000 km^2, which is comparable to the surface of the Gulf of Lion shelf (*ca* 12,000 km^2). Some regions were trawled several times a year, whereas others were

untouched. For strong winds (> 10 m s^{-1}), trawlers were mostly confined to the coastal area, where coarse sediment is more abundant (Fig. 2a). Days of strong winds were present 13% of the year, most of the time in autumn and winter. During low wind periods (≤ 10 m s^{-1}), trawlers preferentially worked on the outer shelf and eroded finer sediment (Fig. 2b). About 2.2×10^4 t of sediment was resuspended daily by bottom trawls (Fig. 9a), with a maximum between September and December 1998 when trawlers were more numerous (> 80, Fig. 3d). The sawtooth pattern is related to the trawling activity that stops weekends and holidays. The annual mass of sediment resuspended by trawling amounted to 5.6×10^6 t (Table 2), most of it originating from depths between 80 and 130 m (Fig. 10). Considering the fraction that settled shortly after resuspension, the annual net erosion/deposition budget on the shelf amounted to 0.4×10^6 t (Table 2), which was one order of magnitude less than that induced by waves- and current-induced resuspension.

The export of resuspended sediment from the shelf showed a seasonal variability, with minimum fluxes during summertime (while the trawling-induced resuspension on shelf was maximum), and a significant increase arising from transport pulses during the winter and spring periods (Fig. 9b). The fine-grained sediment resuspended by trawlers on the outer shelf was exported primarily in the western half of the Gulf (Fig. 10). The off-shelf export added up to 0.4×10^6 t annually, which accounted for ~7% of the quantity of sediment resuspended by trawling on the shelf (Table 2 and Fig. 5).

Transects showed that the cross-slope dispersal of the fine-grained sediment resuspended by trawlers went deeper than for the sediment resuspended by waves and currents, due probably to the proximity of regions of intense trawling activity with the shelf edge. Some sediment settles to depths of 1500-2000 m during summer stratified condition (Fig. 11a). Cascading of dense water during winter caused a rapid advection of turbid shelf water down to 1000 m deep, and settling favoured the spreading of suspended sediment as far as 2000 m deep (Fig. 11b). Above the bottom layer, the dispersal of the suspended particles present in intermediate and deep waters were advected toward the southwest by the general along slope circulation.

Resuspension and off-shelf sediment export induced by both waves/currents and trawls - A simulation with both natural (waves and currents) and anthopogenic (trawling) processes was intended to check if our assumption about the independence on sediment transport was justifiable. By comparison with the sum of both processes, the annual resuspension and deposition on the shelf due to the combined effect of waves/currents and trawls decrease by ~0.17%, and the off-shelf export did not change (Table 2).

The resulting impact of both resuspension processes in the annual change in sediment level is depicted in figure 12. By comparison with the impact of each individual resuspension process (Fig. 7 and 10), the net erosion/deposition intensity is smoothed all over the shelf. The major areas of net erosion appeared along the coast, as well as on the western outer shelf and around the Cape Creus at

the southwestern end of the Gulf. Net sediment accumulation took place over most in the middle shelf and eastern shelf, especially between 20 and 50 m deep.

In the model, trawling-induced resuspension produces over time a slight coarsening of the sediment in the fishing grounds. The impact of bottom trawling activity on the sediment grain size has been already observed elsewhere. Brown *et al.* (2005) showed on the southeastern Bering Sea that an area protected from bottom trawling, but subjected to natural resuspension as the entire coastal region area, had a significantly finer grain size owing to the lack of winnowing impact of trawling-induced resuspension. Thus some synergist effects between natural and trawling resuspensions exist, but they do not significantly change the net erosion and export fluxes for the Gulf of Lion.

5. DISCUSSION

5.1. Comparison of sediment resuspension by waves/currents and trawls

On average, the amount of sediment resuspended by waves and currents exceeds by 3 to 4 orders of magnitude those induced by trawling (Table 2). By calculating the suspended mass per bottom eroded area for annual and winter/summer periods, a comparison can be made between depths eroded by waves and currents, and by trawls (Fig. 13).

Wave and current resuspension flux strongly decreases with increasing water depth, because of the decreasing impact of wave motions, and stabilizes on the outer shelf where strong bottom currents still resuspend muddy sediments (Fig. 13a). Seasonal (winter and summer) fluxes in shallow water are comparable, but summer fluxes decrease more rapidly offshore due to the weaker bottom current intensity. Ulses et al. (this volume) and Dufois et al (this volume) also demonstrate for different periods (2001 and 2003-2004 respectively) that bottom shear stress and sediment erosion was primarily controlled by waves on the inner shelf and by energetic wind-driven currents on the outer shelf.

Resuspension fluxes induced by trawling are maximum on the outer shelf (between 80 and 130 m of depth) and culminate around 100 m depth (Fig. 13b). Seasonally, fluxes are weaker during the winter period by a factor of about 2, because bad sea conditions reduce the average number of sea trips (Fig. 3d). On a yearly basis, resuspension fluxes generated by trawls on the outer shelf are lower than the fluxes generated at the same depths by waves and currents. However, the trawling-induced fluxes significantly exceed the waves and currant-induced fluxes during summertime.

Churchill *et al.* (1989) suggested, using a simple model, that waves and currents on the mid-Atlantic Bight were responsible for the resuspension on the inner shelf shallow water, whereas trawling was the principal cause of resuspension on the outer shelf. Our study shows comparable results and emphasizes the significant impact of bottom trawling on sediment remobilisation in deep regions of

continental shelves. However, the magnitude of the trawling contribution in Churchill's work seems to be significantly greater than the present study. This can be explained by the different methods of calculation, implying a more sophisticated study in the present case. Moreover, sthis discrepancy very likely results from different seafloor characteristics, as the Gulf of Lion shelf is mainly made up of fine sediments (clays and silts), whereas sands primarily dominate the seafloor of the Mid-Atlantic Bight.

5.2. Impact on sedimentary budget

The main export pathways differ for naturally or trawling-induced resuspended sediments because of the different resuspension regions. Waves and currents resuspend sediment mostly on the inner shelf, where it is composed of coarser grains that quickly settle. The fine fraction is then primarily transported along shore toward the southwestern end of the Gulf where it escapes the shelf. Conversely, fine sediment resuspended by trawls is mostly exported to the central slope, owing to the fact that trawled regions are mainly located on the outer shelf, close to the shelf break.

Whereas resuspension induced by waves and currents usually dwarfs that induced by trawling, the net erosion (i.e., resuspension-deposition) and the export are more comparable (Table 2). Indeed, sediments resuspended by trawls contribute to about 5% of the annual total export of riverborne and resuspended sediment Gulf of Lion shelf (Table 2 and Fig. 5). Nevertheless, this export shows an important seasonal and interannual variability due to the storm frequency and intensity, resulting in a variable contribution of trawling to the export.

During summertime the effect of waves and currents is minimal while the activity of trawling is maximum. Quantitatively, these conditions induce an increased contribution of the trawling impact, which reaches 7% of the total export for the period April 1998 - September 1998. During wintertime the contribution of trawling is minimum around 4%.

Ulses *et al.* (submitted) estimated – using a similar modelling approach - a sediment resuspension and export by waves and currents for the Gulf of Lion for the November 2003 - May 2004 period. This latter period was characterized by large river discharges and E-SE storm activity, with the occurrence of one major flood and two extreme storms, but mild dense water formation and export. It was quite different from the low river discharges, low E-SE storm activity, but massive dense shelf water cascading 1998-1999 winter period addressed in the present study. The amount of sediment exported during comparable time period reveals that the export during the November 2003 and March 2004 period (8.6×10^6 t) was larger than during the 1998-1999 period (5.7×10^6 t between November 1998 – March 1999). The 1998-1999 and 2003-2004 periods were very energetic and are believed to represent the upper range of the export. On the other side, Durrieu de Madron *et al.* (2000) estimated from a box model budgeting approach based on direct measurements performed during two seasonal surveys, an annual export of suspended particulate matter of about 1.9×10^6 t. This crude estimate is believed to represent the lower range of the export, as surveys were performed in 1995-1996 during relatively calm conditions. Assuming that the export of sediment associated to the trawling activity is

relatively constant from one year to the other (i.e., of the order of 0.4×10^6 t), we estimated that this activity could contribute between a few and 20 percents of the annual shelf-to-slope exchange of suspended sediment at the scale of the Gulf.

6. CONCLUSIONS

Resuspension and transport of sediment in the Gulf of Lion, due to waves and currents and to trawling, have been modelled for an annual period (April 1998 – April 1999). The major conclusions that can be drawn with these results are:

- Natural resuspension by waves and currents occurred during short episodes mostly during fall and winter. It was concentrated on the inner-shelf due to wave action, but also on the southwestern outer shelf due to the strong bottom currents occurring during wintertime. Trawling-induced resuspension occurred regularly throughout the year. It was concentrated on the outer shelf, with a maximum intensity around 90 m depth. Trawling-induced resuspension fluxes are on average several orders of magnitude lower than the waves and currents-induced resuspension fluxes. Nevertheless, they are maximum and locally predominant during summertime when the wave and currents activity is lowest.

- The total annual off-shelf export of sediment by waves and currents were one order of magnitude larger than the export linked to trawling. Export concerned the finest fraction of the sediment (clays and fine silts) and took place primarily in the southwestern end of the Gulf for the sediment resuspended by waves and currents and the central shelf for the sediment resuspended by trawling. During energetic years (i.e., with large flood, strong marine storm or dense water formation), the trawling activity contributed little (few percents) to the total shelf export of fine sediment. However, trawling was thought to contribute significantly (up to 20% of the export) during calm years.

- No significant interferences between both resuspension processes were estimated in term of resuspension/deposition and export fluxes.

Because of the site-specific characteristics of natural resuspension and transport mechanisms, morphological and sedimentological settings, intensity and distribution of the trawling effort, all the conclusions obtained for the Gulf of Lion may not necessarily apply to other continental shelves. Netherveless, the depth limitation of resuspension by waves and the increasing impact of trawling in deeper portions of the shelf - while natural resuspension processes become tenuous - are likely to be features common to most coastal regions with significant bottom trawling activity.

ACKNOWLEDGMENTS

The authors acknowledge the support from the European Commission (INTERPOL project under contract EVK3-2000-00023 and EUROSTRATAFORM project under contract EVK3-CT-2002-00079). We thank Pat Wiberg and two anonymous reviewers for their constructive and valuable comments.

REFERENCES

Agrawal, Y.C., Pottsmith, H.C. 2000. Instruments for particle size and settling velocity observations in sediment transport. Marine Geology, 168, 89-114

Amos, C.L., Daborn, G.R., Christian H.A. 1992 In situ erosion measurements on fine-grained sediments from the Bay of Fundy. Marine Geology, 108, 175-196.

Amos, C.L., Feeney, T., Sutherland, T.F., Luternauer, J.L. 1997. The stability of fine grained sediments from the Fraser River delta. Estuarine, Coastal and Shelf Science, 45, 507-524.

Arakawa, A. & Suarez, M.J. 1983. Vertical differencing of the primitive equations in sigma coordinates, Monthly Weather Review, 111, 34-45.

Auclair, F., Marsaleix, P., Estournel C., 2000. Sigma coordinate pressure gradient errors : Evaluation and reduction by an inverse method. Journal of Atmospheric and Oceanic Technologies, 17, 1347-1367.

Béthoux, J.P., Durrieu de Madron, X., Nyffeler, F, Tailliez, D. 2002. Deep water in the western Mediterranean : peculiar 1999 and 2000 characteristics, shelf formation hypothesis, variability since 1970 and geochemical inferences. Journal of Marine Systems, 33-34, 117-131.

Black, K.S. 1997. Microbiogical factors contributing to erosion resistance in natural cohesive sediments. In: Burst, N., Parker, R. and Watts, J., Editors. Cohesive sediments, John Wiley & Sons Ltd, Chichester, pp. 231-244.

Blumberg, A.F., Mellor, G., 1987. A description of a three dimensional coastal circulation model, In : Three Dimensional Coastal Ocean Model, edited by N. Heaps, 208 pp.

Bougeault, P., Lacarrere, P. 1989. Parameterisation of orography-induced turbulence in a meso-beta scale model, Monthly Weather Review, 117, pp. 1872-1890.

Bourrin, F., Durrieu de Madron, X., Ludwig, W., 2007. Contribution to the study of coastal rivers and associated prodeltas to sediment supply in Gulf of Lions (N-W Mediterranean Sea). Vie et Milieu. Life and Environment. In press.

Brown E.J., Finney, B., Dommisse, M., Hills, S. 2005. Effects of commercial otter trawling on the physical environment of the southeastern Bering Sea. Continental Shelf Research, 25, 1281-1301.

Canals, M., Puig, P., Durrieu de Madron, X., Heussner, S., Palanques, A., Fabrè J. 2006. Flushing submarine canyons. Nature, 444, 354-357.

Churchill, J.H. 1989. The effect of commercial trawling on sediment resuspension and transport over the Middle Atlantic Bight continental shelf. Continental Shelf Research, 9, 841-864.

DeAlteris, J., L. Skrobe and C. Lipsky. 1999. The significance of seabed disturbance by mobile fishing gear relative to natural processes: a case study in Narragansett Bay, Rhode Island. In L.R. Benaka, editor. Fish Habitat: Essential fish habitat and rehabilitation. American Fisheries Society, Symposium 22, Bethesda, Maryland, 224-237

Dufau-Julliand, C., Marsaleix, P., Petrenko, A., Dekeyser, I. 2004. 3D modeling of the Gulf of Lion's hydrodynamics (NW Med.) during January 1999 (MOOGLI3 experiment) and late winter 1999 : WIW formation and cascading over the shelf break. Journal of Geophysical Research.109, C11002, doi:10.1029/203JC002019.

Durrieu de Madron, X., Nyffeler, F., Godet, C.H. 1990. Hydrographic structure and nepheloïd spatial distribution in the Gulf of Lions continental margin. Continental Shelf Research, 10, 915-929.

627 Durrieu de Madron, X., Abassi, A., Heussner, S., Monaco, A., Aloisi, J.C., Radakovitch, O., Giresse,
628 P., Buscail, R., Kerhervé, P. 2000. Particulate matter and organic carbon budgets for the Gulf of Lions
629 (NW Mediterranean). Oceanologica Acta, 23 (6), 717-730

630 Durrieu de Madron, X., Denis, L., Diaz, F., Garcia, N., Guieu, C., Grenz, C., Loÿe-Pilot, M.D., Ludwig,
631 W., Moutin, T., Raimbault, P., Ridame, C. 2003. Nutrients and carbon budgets for the Gulf of Lion
632 during the Moogli cruises. Oceanologica Acta, 26, 421-433.

633 Durrieu de Madron X., Ferré, B., Le Corre, G., Grenz, C., Conan, P., Pujo-Pay, M., Bodiot, O., Buscail,
634 R. (2005) Trawling-induced resuspension and dispersal of muddy sediments and dissolved elements.
635 Continental Shelf Research, 25 (19-20), 2387-2409.

636 Dyer, K.R. 1986. Coastal and Estuarine Sediment Dynamics, John Wiley and Sons, London.

637 El Ganaoui O., Schaaff E., Boyer P., Amielh M., Anselmet F. and Grenz C. (2004) The deposition and
638 erosion of cohesive sediments determined by a multi-class model. Estuarine, Coastal and Shelf
639 Science, 60 (3), 457-475

640 Estournel, C., Kondrachoff, V., Marsaleix, P., Vehil, R. 1997. The plume of the Rhône : numerical
641 simulation and remote sensing, Continental Shelf Research, 17, 899-924.

642 Estournel, C., Broche, P., Marsaleix, P., Devenon, J.L., Auclair, F., Vehil, R. 2001. The Rhone river
643 plume in unsteady conditions : numerical and experimental results. Estuarine, Coastal and Shelf
644 Science, 53, 25-38.

645 Estournel, C., Durrieu de Madron, X., Marsaleix, P., Auclair, F., Julliand, C., Vehil, R. 2003.
646 Observations and modelisation of the winter coastal oceanic circulation in the Gulf of Lions under wind
647 conditions influenced by the continental orography (FETCH experiment). Journal of Geophysical
648 Research, 108(C3), p. 8059.

649 Ferré, B., Guizien, K., Durrieu de Madron, X., , Palanques, A., Guillén, J., Grémare, A. 2005.Fine
650 sediment dynamics study during a winter storm in the Gulf of Lion shelf (NW Mediterranean), en
651 révision à Continental Shelf Research. Continental Shelf Research, 25 (19-20), 2410-2427.

652 Garcia-Estevez, J. 2005. Transferts géochimiques en Méditerranée : exemple de la rivière Têt et de
653 son bassin versant. Ph.D. Thesis, University of Perpignan, pp 263.

654 Geernaert, G.L. 1990. Bulk parameterizations for the wind stress and heat fluxes. In: Geenaert and
655 Plant (Eds.), Surface waves and fluxes. Volume I -Current theory. Kluwer Academic Publishers, pp.
656 336.

657 Grant, W.D., Madsen, O.S., 1982. Movable bed roughness in unsteady oscillatory flow. Journal of
658 Geophysical research, 87, 469-481.

659 Guillén J., Bourrin, F., Palanques, A., Durrieu de Madron, X., Puig, P., Buscail, R. 2006. Sediment
660 dynamics during “wet” and “dry” storm events on the Têt inner shelf (SW Gulf of Lions). Marine
661 Geology, 234, 129-142.

662 Gust, G., Morris, M.J. 1989. Erosion thresholds and entrainment rates of undisturbed in situ
663 sediments. Journal Coastal Research, 5, 87-99.

664 Harris, C.K, Wiberg, P.L. 2001. A two-dimensional, time-dependent model of suspended sediment
665 transport and bed reworking for continental shelves. Computers and Geosciences, (27), 675-690.

666 Heussner S., Durrieu de Madron, X., Calafat, A., Canals, M., Carbonne, J., Delsaut, N., Saragoni, G.,
667 2006. Spatial and temporal variability of downward particle fluxes on a continental slope: lessons from
668 an 8-yr experiment in the Gulf of Lions (NW Mediterranean). Marine Geology, 234, 63-92

669 Hill, P.S., Syvitski, J.P., Cowan, E.A., Powell, R.D., 1998. Insitu observations of floc settling velocities
670 in Glacier Bay, Alaska. Marine Geology, 145, 85-94.

671 Houwing, E.J. 1999. Determination of the critical erosion threshold of cohesive sediments on intertidal
672 mudflats along the Dutch Wadden sea coast. Estuarine, Coastal and Shelf Science, 49, 545–555.

673 Houwing, E.J. 2000. Sediment dynamics in the pioneer zone in the land reclamation area of the
674 Wadden Sea, Groningen, The Netherlands. Ph.D. Thesis, University of Utrecht, Utrecht.

675 Krishnappan, B.G., Marsalek, J., 2002. Transport characteristics of fine sediment from an on-stream
676 stormwater management pond. Urban Water, 4, pp. 3-11.

677 Lapouyade, A., Durrieu de Madron, X., 2001. Seasonal variablility of the advective transport of
678 particulate matter and organic carbon in the Gulf of Lion (NW Mediterranean). Oceanologica Acta, 24,
679 295-312.

680 Li, M.Z., Amos, C.L. 1998. Predicting ripple geometry and bed roughness under combined waves and
681 currents in a continental shelf environment. Continental Shelf Research, 18(9), 941-970.

682 Li, M.Z., Amos, C.L. 2001. SEDTRANS96 : the upgraded and better calibrated sediment-transport
683 model for continental shelves. Computers and Geosciences, (27), 619-645.

684 Maa, J.P., Sanford, L., Halka, J.P. 1998. Sediment resuspension characteristics in Baltimore Harbor,
685 Maryland. Marine Geology, 146, 137-145

686 Marsaleix, P., Estournel, C., Kondrachoff, V., Vehil, R. 1998. A numerical study of the formation of the
687 Rhone river plume. Journal of Marine Systems, 14, 99-115.

688 Meadows, P.S., Tait, J., Hussain, S.A. 1990. Effects of estuarine infauna on sediment stability and
689 particle sedimentation. Hydrobiologia, 190, 263-266.

690 Millot, C., 1999. Circulation in the western Mediterranean Sea. Journal of Marine Systems, 20 (1-4),
691 423-442.

692 Monaco, A., Durrieu de Madron, X., Radakovitch, O., Heussner, S. & Carbonne, J. 1999. Origin and
693 variability of downward biogeochemical fluxes on the Rhône continental margin (NW Mediterranean). -
694 Deep-Sea Research I, 46, 1483-1511.

695 Mulder, H.P., Udink, C. 1991. Modelling of cohesive sediment transport. A case study: the western
696 Scheldt estuary. In: Edge, B.L. Editor. Proceedings of the 22nd International Conference on Coastal
697 Engeneering, ASCE, 3012-3023.

698 Nielsen, P. 1986. Suspended sediment concentrations under waves. Coastal Engeneering, 10, 23-31?

699 Oey, L.Y., Chen, P. 1992. A model simulation of circulation in the northeast Atlantic shelves and seas.
700 J. Geophys. Res., 97, 20,087-20,115

701 Palanques, A., Durrieu de Madron, X., Puig, P., Fabres, J., Guillén, J., Calafat A., Canals, M.,
702 Heussner, S., Bonnin, J. 2006. Suspended sediment fluxes and transport processes in the Gulf of
703 Lions submarine canyons. The role of storms and dense water cascading. Marine Geology, 234, 43-
704 61.

705 Palanques, A., Puig, P., Guillén, J., Jiménez, J., Gracia, V., Sánchez-Arcilla, A. and Madsen, O.
706 2002. Near-bottom suspended sediment fluxes on the microtidal low-energy Ebro continental shelf
707 (NW Mediterranean) Continental Shelf Research, 22, 285-303.

708 Panagiotopoulos, I., Voulgaris, G., Collins, M.B. 1997, The influence of clay on the threshold of
709 movement on fine sandy beds, Coastal Engineering, 32, 19-43.

710 Partheniades, E. 1962. A study of erosion and deposition of cohesive soils in salt water. Ph. D. Thesis.
711 University of California, Berkeley, 182 pp.

712 Pethelet-Giraud, E., Negrel, P.-H., Cubizolles, J., 2003. Flux exportés de l'Hérault vers la
713 Méditerranée et origine des masses d'eau. Rapport BRGM /RP-52748-FR.

714 Petrenko, A., Leredde, Y., Marsaleix, P., 2004. Circulation in a stratified and wind-forced Gulf of Lions,
715 NW Mediterranean Sea: in situ and modelling data. Continental Shelf Research, 25 (1), 7-27.

716 Poirel, A., Carrel, G., Olivier, J.M., 2001. Illustration de la complémentarité des chroniques
717 environnementales dans l'étude d'un hydrosystème fluvial : régime thermique et peuplements
718 piscicoles du Rhône, Workshop "Activities in the catchment area and water quality", Lyon Fleuves
719 2001, juin 2001.

720 Schaaff, E., Grenz, C., Pinazo, C., 2002. Erosion of particulate inorganic and organic matter in the
721 Gulf of Lion. Comptes Rendus Géosciences, 334, 1071–1077.

722 Sempéré R., Charrière B., Van Wambeke F. and Cauwet G. (2000) Carbon inputs of the Rhone River
723 to the Mediterranean Sea: Biogeochemical implications. Global Biogeochemical Cycles, 14, 669-681.

724 Serrat, P. 1999. Present sediment yield from a Mediterranean fluvial system: the Agly river (France).
725 Comptes Rendus de l'Académie des Sciences - Series IIA - Earth and Planetary Science. 329,189-
726 196.

727 Serrat, P., Ludwig, W., Navarro, B., Blazi J.L., 2001. Spatial and temporal variability of sediment fluxes
728 from a coastal Mediterranean river: the Têt (France). Comptes Rendus de l'Académie des Sciences -
729 Series IIA - Earth and Planetary Science, 333, 389-397.

730 Soulsby, R.L., Hamm, L., Klopman, G., Myrhaug, D., Simons, R.R., Thomas G.P. 1993. Wave-current
731 interaction within and outside the bottom boundary layer. Coastal Engeneering, 21, 41-69.

732 Soulsby, R.L., Whithouse, R.J.S.W. 1997. Threshold of sediment motion in coastal environments.
733 Proceedins Pacific Coasts and Ports '97 Conference, Christchurch, 1, 149-154.

734 Torfs, H. 1995, Erosion of mud/sand mixtures. Ph.D. thesis, Katholieke Universiteit Leuven, faculteit
735 der Toegepaste Wetenschappen, Departement Burgelijke Bouwkunde, Laboratorium voor Hydraulica.

736 Ulses, C., Estournel, C., Bonnin, J., Durrieu de Madron, X., Marsaleix, P. Impact of storms and dense
737 water cascading on shelf-slope exchanges in the Gulf of Lion (NW Mediterranean). Journal of
738 Geophysical Research (accepted).

739 Ulses, C., Estournel, C., Durrieu de Madron, X., Palanques, A. Suspended sediment transport in the
740 Gulf of Lion (NW Mediterranean) : Impact of extreme flood and storm. Continental Shelf Research
741 (submitted)

742 Wentworth, C.K. 1922. A scale of grade and class terms for clastic sediments, Journal of Geology, 30,
743 377-392.

744 Wheatcroft, R.A. 1994. Temporal variation on bed configuration and one–dimensional bottom
745 roughness at the mid-shelf STRESS site. Continental Shelf research, 14, 1167-1190.

746 Widdows, J., Brinsler, M.D., Bowley, N., Barrett C., 1998. A benthic annualar flume for in situ
747 measurement of suspension feeding/biodeposition rates and erosion potential of intertidal cohesive
748 sediments. Estuarine, Coastal and Shelf Sciences, 46, 27-38.1998

749 Zanke, U. 1977. Berechnung der Sinkgeschwindichkeiten von Sedimenten. Mitteilungen des Franzius-
750 Institutes, 46, 231-245.

751 Zyserman, J.A., Fredsøe, J., 1994. Data analysis of bed concentration of suspended sediment.
752 Journal of Hydraulic Engineering, ASCE, 120 (9), 1021-1041.

753

APPENDIX 1

Suspended sediment transport equation

The advection-diffusion equation is based on the mass conservation of the suspended sediment

$$\frac{\partial C^i}{\partial t} + u\frac{\partial C^i}{\partial x} + v\frac{\partial C^i}{\partial y} + \left(w - W_s^i\right)\frac{\partial C^i}{\partial z} = K_z\frac{\partial^2 C^i}{\partial z^2} \quad (1)$$

where C^i is the suspended sediment concentration (SSC) for the i^{th} class of particles, W_s^i is the settling velocity, u, v and w are the horizontal and vertical velocity respectively and K_z is the vertical diffusion coefficient.

The vertical turbulence was estimated using a turbulent closure scheme where the vertical diffusion coefficient K_z is derived from the local Richardson number $\left(Ri = -\frac{(g/\rho)(\partial\rho/\partial z)}{(\partial u/\partial z)^2}\right)$:

$$K_z = 1.67\times10^{-3}\left(1+\frac{10}{3}Ri\right)^{-3/2} \quad (2)$$

where ρ is the water density and g is the gravitational acceleration equal to 9.81 $m^2\ s^{-1}$.

Settling velocity W_s^i (in $m\ s^{-1}$) for the particles with a diameter lower than 100 µm was estimated as the mean Stokes velocity of the individual size bins D_j (in m):

$$W_s^i = \frac{(s_i - 1)gD_i^2}{18\nu} \quad (3)$$

where s_i is the relative grain density and ν is the kinematic water viscosity equal to 1.14×10^{-6} $m^2\ s^{-1}$.

Settling velocity for sand grain coarser than 100 µm is computed using Zanke (1977) formula:

$$W_s^i = \frac{10\nu}{D_i}\left\{\left[1+\frac{0.01(s_i-1)gD_i^3}{\nu^2}\right]^{0.5} - 1\right\} \quad (4)$$

770 Settling velocity of aggregates is computed using the relationship from Agrawal and Pottsmith (2000):

$$W_s^i = 0.45\times10^{-3}\left(D_i/2\right)^{1.17} \quad (5)$$

771 where W_s^i and D_i are expressed in cm s^{-1} and µm respectively.

772

773 Density of primary particles is taken as the mineral grain density (2640 kg m^{-3}) and density of
774 aggregates is calculated according to Hill *et al.* (1998):

$$\rho_f^i = \rho + \frac{18\mu W_s}{gD_f^2}\left(1+\frac{3C}{16}\mathrm{Re}\right) \quad (6)$$

775 where ρ_f^i is the aggregate density, μ is the dynamic water viscosity (1.14×10^{-3} kg m^{-1} s^{-2}), W_s is the
776 aggregate settling velocity, D_f is the aggregate diameter, C is the Carrier coefficient (0.43) and
777 $\mathrm{Re} = \rho W_s^i D_f^i / \mu$ is the class i Reynolds number.

778

APPENDIX 2

Erosion flux for trawl

The fluxes of sediment resuspended by bottom trawls were estimated experimentally and presented in Durrieu de Madron *et al.* (2005). By comparing resuspension by two different configurations of groundrope gear (chain or "rock hopper" fixed rubber discs), working at a speed of 3 knots over the ground, with an average net aperture and door width of 16 m, they showed that resuspension by trawl depend on the trawl's goundrope, but above all on the sediment texture (clay content). A linear relationship is inferred between the total resuspension flux, E_T in kg m^{-2} s^{-1}, and the clay fraction, F_C in %:

$$E_T = 0.011\,F_C + 0.47 \quad (r^2 = 0.74)$$

Total flux is then fractionated for the different sediment grain sizes, according to the fraction p_i of class *i*.

$$F^i = p_i\,E_T$$

Erosion fluxes for waves and currents

Partheniades' law for cohesive sediments - It permits to calculate the erosion flux *F* for each particle class *i* according to the relation:

$$F^i = p_i E_0^i \left(\frac{\tau_{\max,s}}{\tau_{cr_i}} - 1 \right) \text{ if } \tau_{\max,s} \geq \tau_{cr_i} \qquad (7)$$

where τ_{cr_i} is the critical shear stress for the class *i* and p_i is the fraction of class *i*. The erosion coefficient E_0 depends on the physico-chemical sediment characteristics and ranged between 10^{-5} and $2\ 10^{-3}$ kg m^2 s^{-1} (Mulder et Udink, 1991; Amos *et al.*, 1992; Amos *et al.*, 1997, Widdows *et al.*, 1998). In this study, the coefficient E_0 was set to $1\ 10^{-5}$ kg m^2 s^{-1}

Reference concentration method for non-cohesive sediments – It permits to calculate the erosion flux *F* for each particle class *i* according to the relation:

$$F^i = p_i W_s^i C\left(z_1\right) \rho_s^i \quad (8)$$

where $C(z_1)$ is an adimensional concentration at the height z_1 corresponding to the first layer of the grid of above the seabed. Under combined wave and currents conditions, sediment is resuspended within the wave boundary layer and diffused in the water column by turbulence associated with the current (Soulsby *et al.*, 1993). In the model, height of the first layer (z_1) is variable and can be above the wave boundary layer of thickness z_w. The concentration $C(z_1)$ is thus calculated according to the reference concentration C_a, at height $z_a=2D_{50}$, or the concentration at the boundary layer level $C(z_w)$.

$$C(z_1) = C_a \left(\frac{z_1}{z_a} \right)^{-b_{\max}} \quad \text{for } z_a \le z_1 \le z_w$$

$$C(z_1) = C(z_w) \left(\frac{z_1}{z_w} \right)^{-b_m} \quad \text{for } z_w < z_1$$

$$\text{with} \quad b_{\max} = \frac{W_s}{\kappa u_{*\max}} \text{ and } \quad b_{\mathrm{m}} = \frac{W_s}{\kappa u_{*\mathrm{m}}}$$

$$z_w = \frac{u_{*\max} T}{2\pi} = \text{wave boundary thickness}$$

W_s is the sediment settling velocity, κ is the von Karman constant (= 0.40), $u_{*max} = (\tau_{max} / \rho)^{1/2}$, $u_{*m} = (\tau_m / \rho)^{1/2}$, τ_{max} is the maximum bed shear-stress in wave cycle, τ_m is the mean bed shear-stress in wave cycle, and T the wave period.

The determination of the reference concentration is based on Zyserman and Fredsøe (1994) method, and is calculated for a grain-related roughness height of $2.5 \times D_{50}/30$:

$$C_a = \frac{0.331\,(\theta_{\max,s} - 0.045)^{1.75}}{1 + 0.720\,(\theta_{\max,s} - 0.045)^{1.75}} \quad (9)$$

Where $\theta_{\max,s} = \dfrac{\tau_{\max,s}}{g(\rho_s - \rho) D_{50}}$ is the skin-friction Shields parameter.

The latter method is designed for flat-bed condition, so that τ_{max} and τ_m are calculated using a grain related roughness height $\left(2.5 \times D_{50}/30\right)$. For a rippled bed, total-stress values should be used.

Critical shear stress

The critical shear stress is the shear stress from which sediment is likely to be removed. It depends on the grain itself and on bottom characteristics. This value is difficult to establish because it can vary from a factor 10 to 20 according to the type of resuspension considered.

For coarse non-cohesive sediments which mainly depend on grain characteristics, critical shear stress of each class i is given in form of a critical Shields parameter value θ_{cr}^i which depends on

822 adimensional grain size and results from experiments. Soulsby and Whithouse (1997) determined an
823 algebraic equation nearest to the Shields curve:

$$\theta_{cr}^{i} = \frac{0.30}{1+1.2D_{*}^{i}} + 0.055\left[1-e^{-0.020D_{*}^{i}}\right] \text{ where } D_{*}^{i} = \left[\frac{g(s^{i}-1)}{\nu^{2}}\right]^{1/3} D_{50}^{i} \quad (10)$$

824 Critical shear stress τ_{cr}^{i} is thus calculated with the equation

$$\theta_{cr}^{i} = \frac{\tau_{cr}^{i}}{g\left(\rho_{s}^{i}-\rho\right)D_{50}^{i}} \quad (11)$$

825

826 *Roughness and bedforms*

827 For non-cohesive sediments, total bottom roughness is computed using the relationship

$$z_0 = k/30 \quad (12)$$

828 where *k* is the total roughness height, and is the sum of three components: grain-related component
829 (k_g), bedload component (k_t), and form-drag component (k_f) (Grant and Madsen, 1982).

$$k = k_g + k_t + k_f \quad (13)$$

830 Grain roughness height is calculated using:

$$k_g = 2.5 \times D_{50} \quad (14)$$

831 Bedload roughness is calculated using:

$$k_t = 522 \times D_{50}\left(\theta_{cws} - \theta_{cr}\right)^{0.75} \quad (15)$$

832 where $\theta_{cws} = \rho u_{*cws}^{2} / \left(\rho_s - \rho\right) g D_{50}$ is the Shields parameter related to the skin roughness, θ_{cr} is the
833 critical Shields parameter which define grains remobilization, and U_{*cws} is combined wave and currents
834 shear velocities.
835 The ripple height and wavelength is then calculated according to Li and Amos (1998) (see below) to
836 obtain the form drag roughness height
837

$$k_f = a_r \eta^{2} / \lambda \quad (16)$$

where a_r is a coefficient which varies according to authors. We choose 27.7, the most common value, fixed by Grant and Madsen (1982).

The ripple height and wavelength depend on the characteristic and hydrodynamical conditions. Skin shear velocities (u^*_{cws}) and skin-friction combined wave and current Shields parameter (θ_{cws}) are first calculated using the grain roughness height k_g. The bedload roughness k_t can thus be calculated, and is used to obtain bedload shear velocities (u^*_{wt}, u^*_{ct}, u^*_{cwt}). To calculate ripples dimension, the combined-flow ripple predictor proposed by Li and Amos (1998), based on their filed observations of ripples on Scotian Shelf, is used. Ripple dimensions are calculated according to five limit condition for friction velocities: ripple-enhanced shear velocity (u_{*cwe}, Nielsen, 1986), critical shear velocity for bedload transport (u_{*cr}), critical shear velocity for ripple break-off (u_{*bf}, Grant and Madsen, 1982) and critical shear velocity for upper-plane bed sheet-flow (u_{*up}). This last variable is given from a data compilation from preceding studies, carried out by Li and Amos (1998).

$u_{*cwe} = u_{*cws} \Big/ \left(1 - \pi \eta_p / \lambda_p\right)$ where η_p and λ_p are respectively height and wavelength of pre-existing ripples.

$u_{*cr} = \sqrt{\tau_{cr} / \rho}$, τ_{cr} being the critical shear stress for erosion as explain hereafter.

$u_{*bf} = 1.34\, S_*^{0.3}\, u_{*cr}$ where $S_* = (D_{50} / 4\nu)\left[\left(\rho_s - \rho\right) g\, D_{50} / \rho\right]$ is without dimension and ν is the cinematic seawater viscosity (equal to 1.14×10^{-6} for a 15°C seawater).

$u_{*up} = \sqrt{\tau_{up} / \rho}$ where $\tau_{up} = \theta_{up}\left(\rho_s - \rho\right) g\, D_{50}$ and $\theta_{up} = 0.172 D_{50}^{-0.376}$, D_{50} is expressed in mm.

The five limit conditions are presented above and permit to determine the adapted equations to calculate ripples height η_{rip} and wavelength λ_{rip} :

- If $u_{*cwe} < u_{*cr}$, there is no sediment transport and ripples have the same dimension as precedent time step.

- If $u_{*cwe} > u_{*cr}$ and $u_{*cws} < u_{*cr}$, the transport is local, weak, and close to ripples crest.

  - η_{rip} / D_{50} =19.59 (u_{*cws} / u_{*cr}) + 20.92
  - $\eta_{rip} / \lambda_{rip}$ = 0.12

- If $u_{*cws} > u_{*cr}$ and $u_{*cwt} < u_{*bf}$, overall bedload transport will occur.

  <u>*case n°1*</u> *:* $u_{*cw} / u_{*cs} \geq 1.25$, wave-dominant ripples

  - η_{rip} / D_{50} =27.14 (u_{*cwt} / u_{*cr}) + 16.36
  - $\eta_{rip} / \lambda_{rip}$ = 0.12

  <u>*case n°2*</u> *:* $u_{*cw} / u_{*cs} < 1.25$, current-dominant ripples or interaction between wave and currents

  - η_{rip} / D_{50} =22.15 (u_{*cwt} / u_{*cr}) + 6.38

869 o $\eta_{rip} / \lambda_{rip} = 0.12$

870 - If $u_{*bf} \leq u_{*cwt} < u_{*up}$, break-off ripples will form

871 - $\lambda_{rip} = 535\ D_{50}$

872 - $\eta_{rip} / \lambda_{rip} = 0.15\ (u_{*up} - u_{*cwt}) / (u_{*up} - u_{*bf})$

873 - If $u_{*cwt} \geq u_{*up}$, ripples are washed out and upper-plane bed will be predicted.

874 - $\eta_{rip} = 0$

875 - $\lambda_{rip} = 0$

876 From these ripples height and wavelength values, the drag roughness, and then the total bottom
877 roughness can be calculated, giving access to the calculation of the bottom shear stress which will
878 determine the reference concentration.

879

880 For cohesive sediment, biological activity can have a considerable effect on bottom roughness.
881 Microbial exudates can increase the critical shear stress, and presence of burrows in the sediment,
882 due to bioturbation, can strengthen the seabed (Meadows *et al.*, 1990; Black, 1997). Data concerning
883 biological roughness being non-existent in the Gulf of Lion, ripples height and the wavelength for
884 3.6cohesive sediment are selected here equal to those measured on a silty site in the North-East of
885 California, that says 0.6 cm and 10 cm respectively (Wheatcroft, 1994). The steepness of biogenic
886 roughness elements is assumed to decay under high shear stresses as:

$$\frac{\eta_{bio}}{\lambda_{bio}} = \exp\left(-1.67 \ln \theta_w - 4.11\right) \text{ (Harris and Wiberg, 2001)} \quad (17)$$

887 where $\theta_w = \tau_{*w} / g(\rho_s - \rho) D_{50}$.

888 For mixed sediment, an average between silty-bed and sandy-bed roughness scale is used, weighted
889 by sand fraction of the bed (Harris et Wiberg, 2001) :

$$\begin{aligned} \eta &= \eta_{rip}\, fr_s + \eta_{bio}\left(1 - fr_s\right) \\ \lambda &= \lambda_{rip}\, fr_s + \lambda_{bio}\left(1 - fr_s\right) \end{aligned} \quad (18)$$

890 where f_{rs} is the sandy fraction. In the same way, total roughness is calculated by weighted average of
891 the cohesive and non-cohesive contributions. A minimum value of z_0=0.005 cm is specified so that
892 roughness estimates do not become too small given the small-scale bed variations generally present
893 on the sea floor.

894

895 *Bed armoring*

896 We used the method of Harris and Wiberg (2001), which considers several layers below an active
897 layer available for erosion. Underlying layers are only available when active layer gets thinner by
898 erosion or when shear stress increases. At the initial time, all layers (under-layers and active layer)
899 have the same particle size distribution. The thickness and particle size distribution of each layer are
900 updated at each time step according to deposit and erosion. Volume of each particles class per unit
901 area of eroded seabed during a time step is limited by the quantity of sediment available in the active
902 layer.

903 The active layer of sandy bottom (δ^{rip}) is calculated according to the migration rate of the bottom (Q_b)
904 and the size of the ripples η_{rip} and λ_{rip} during a half wave-period:

$$\delta^{rip} = \frac{Q_b\, T}{2C_b \lambda_{rip}} + 6D_{50}$$
$$\text{where } Q_b = \sum_i \left[fr_i \frac{25.3}{\left(\rho_s^i - \rho\right) g} \left(\tau_{cws} - \tau_{cr}^i\right)^{1.5} \right] \text{ and } \tau_{cws} = \rho u_{*cws}^2 \qquad (19)$$

905 where fr_i is the fraction of class i present in the sediment, C_b is the concentration of the sediment (1-
906 porosity), and $6D_{50}$ represents irregularities due to grains in order to prevent the active layer to
907 disappear when no transport occurs.

908 For silty sediments, the active layer depth is supposed to be proportional to the shear stress at the
909 bottom compared to the critical shear stresses $\tau_{cr(50)}$ of the sediment.

$$\delta^{silt} = 0.006\left(\tau_{cws} - \tau_{cr(50)}\right) + 6D_{50} \qquad (20)$$

910

911 For mixed sediment (mixture of silt and sand), the mixed layer δ_{mix} is calculated as a weighted mean of
912 active layer depths for sandy and silty sediments.

$$\delta_{mix} = \delta^{rip}\, fr_s + \delta^{silt}\left(1 - fr_s\right) \qquad (21)$$

913 where fr_s is the sand fraction of the bed. Volume of sediment available for erosion in a size class i per
914 unit area of the bed is $fr_i C_b \delta_{mix}$. This volume is used to limit the erosion, taking into account initial
915 sediment characteristics (critical shear stress for erosion, grain density and particle size distribution).
916 Hence, when erosion exceeded the available sediment volume for each class i at a given site, bed
917 armoring is applied by reducing the flux of this class.

FIGURES CAPTIONS

Figure 1. (a) Bathymetry of the Gulf of Lion in the model and position of hydrological stations. The thick dashed line around the shelf break depth (200 m) delineates the limit between the shelf and the open sea. Stars near the coast and within canyon heads represent the location of the bottom-shear stress estimates (Fig. 3e) and near-bottom density anomaly estimates (Fig. 3 f). The shelf is subdivided in two halves (cross shelf thin dashed line) for water flux estimates given in Fig. 3g. (b) Median grain size of superficial sediment showing the seaward fining texture of the sediment and coarsening around the shelf edge.

Figure 2. Probability density distribution of bottom trawls for a) weak wind ($\leq$ 10 m s^{-1}) and b) strong winds (>10 m s^{-1}). Black dots indicate the position of fishing ports sheltering the fleet of bottom trawlers: PV (Port-Vendres), PN (Port-la-Nouvelle), A (Agde), S (Sète), GR (Grau du Roi), PB (Port de Bouc). Isobaths 50, 200, 1000 and 2000 m superimposed as black lines.

Figure 3. Time series from April 1998 to April 1999 of (a) water discharges from the Rhône River and other rivers of the Gulf of Lion, (b) solid discharge from all rivers, (c) wind off Sète, (d) daily strength of bottom trawls in the Gulf of Lion, (e) bottom shear stress off Marseille and Banyuls (see Fig. 1 for position), (f) water density anomaly at 200 m depth at the eastern end (Planier Canyon) and southwestern end (Cape Creus Canyon) of the Gulf, and (g) and water flux across the shelf break (slope water import onto the shelf is positive, whereas shelf water export is negative).

Figure 4. Map of sediment thickness accumulated after a 16-month simulation (January 4, 1998 – March, 31, 1999) taking solely into account sediment discharges from rivers (no resuspension allowed).

Figure 5. Cumulative export (in 10^6 Tons) for the different scenarios: a) natural (waves and currents), b) trawls and c) mixed (waves, currents, and trawls). The dotted line indicates the sum of export for scenarios (a) and (b).

Figure 6. Annual (from April 1, 1998 to March 31, 1999) variability of the mass of sediment resuspended daily by waves and currents on the shelf (a) and exported towards the slope (b).

Figure 7. Map of sediment thickness accumulated or eroded between April 1, 1998 and March 31, 1999 taking into account sediment discharges from all rivers and resuspension by waves and currents. The contours are in mm, positive values (light areas) represent deposition and negative values (dark areas) represent erosion.

Figure 8. Cross-margin sections on the western part of the Gulf of Lion (see Fig. 1 for section position) showing the distribution of suspended sediment concentration, resuspended by waves and currents, along with water density anomaly in (a) strongly stratified conditions (27 September 1998), and (b)

951 weakly stratified conditions (24 February 1999). The contour unit is mg L^{-1}. The inserted map indicates
952 the location of the cross-slope transect.

953 Figure 9. Annual (from April 1, 1998 to March 31, 1999) variability of the mass of sediment
954 resuspended daily by bottom trawlers on the shelf (a) and exported towards the slope (b). Trawling
955 activity occurs every day but during weekends and holidays.

956 Figure 10. Map of sediment thickness accumulated or eroded between April 1, 1998 and March 31,
957 1999 taking into account sediment discharges from all rivers and resuspension by bottom trawling.
958 The contours are in mm, positive values (light areas) represent deposition and negative values (dark
959 areas) represent erosion.

960 Figure 11. Cross-margin sections on the western part of the Gulf of Lion (see Fig. 1 for section
961 position) showing the distribution of sediment concentration, resuspended by bottom trawling, along
962 with water density anomaly in (a) strongly stratified conditions of the upper layer of the water column
963 (27 September 1998), and (b) weakly stratified conditions (24 February 1999). The contour unit is mg
964 L^{-1}. The inserted map indicates the location of the cross-slope transect.

965 Figure 12. Annual and seasonal variation with depth of the temporally integrated resuspension fluxes
966 on the Gulf of Lion's shelf linked (a) to natural (wave and current) activity, and (b) to bottom trawling
967 activity. The first 30 m depths are not represented because of the strong erosion by waves and
968 currents very near the coast which dwarfed the other values.

969 Figure 13. Map of sediment thickness accumulated or eroded between April 1, 1998 and March 31,
970 1999 taking into account sediment discharges from all rivers and both resuspension by waves and
971 currents, and bottom trawling. The contours are in mm, positive values (light areas) represent
972 deposition and negative values (dark areas) represent erosion.

973 **TABLE CAPTIONS**

974 Table 1. Characteristics of particle grain size classes used in the sediment transport model.

975 Table 2. Annual sediment fluxes integrated between April 1, 1998 and March 31, 1999. Scenarios with
976 natural (waves and currents) and/or trawling resuspension include sediment input by rivers. Deposition
977 and export rates for these scenarios exclude the deposited and exported sediment directly deriving
978 from rivers. Once riverine sediment has been deposited on the shelf it is accounted in the
979 resuspension, and subsequent deposition and export fluxes.

980

981

982

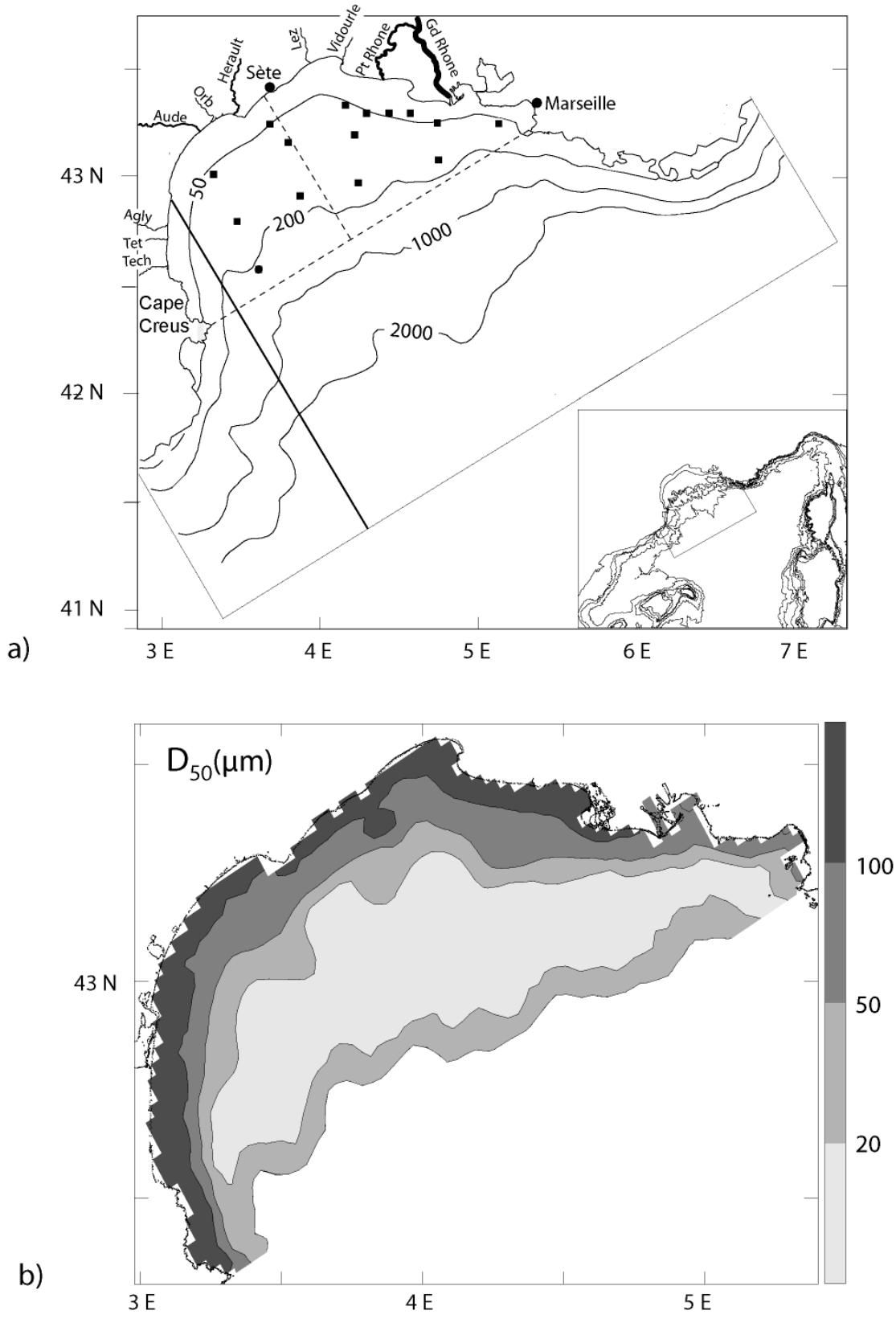

Ferre et al. Figure 1

983

984

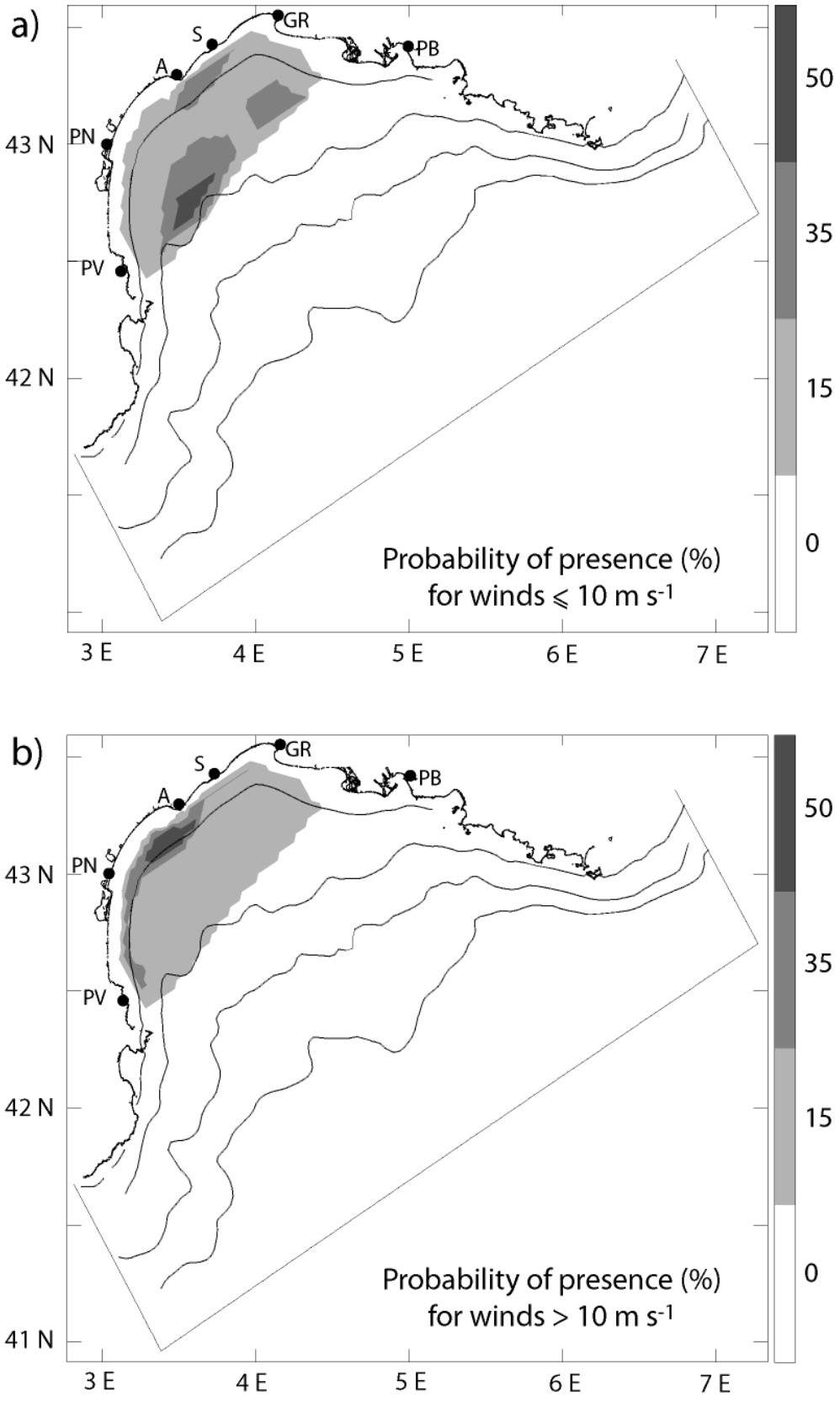

985 Ferre et al. Figure 2

986

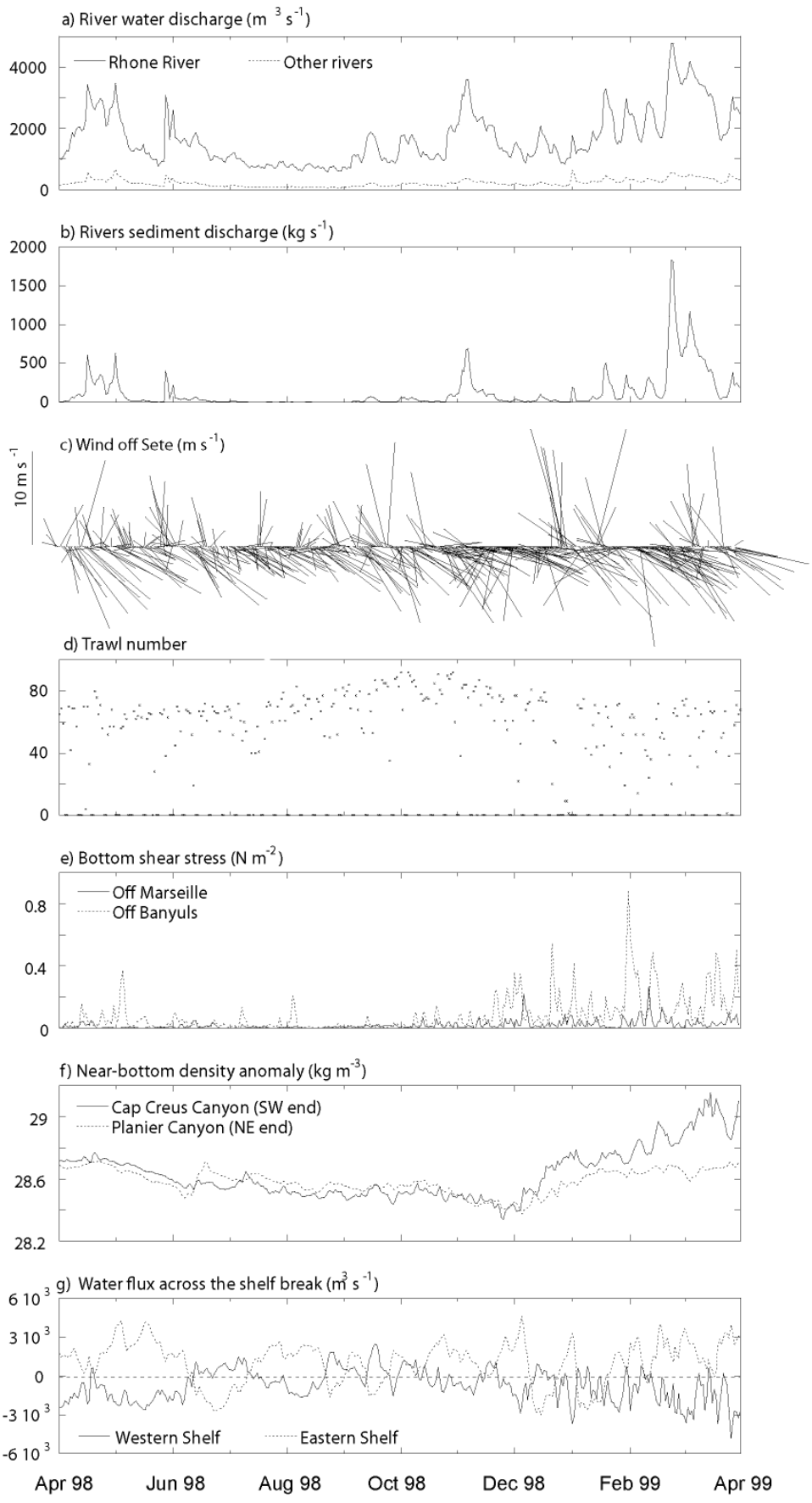

987

Ferre et al. Figure 3

988

989

990

991

992

993

994

995

996

997

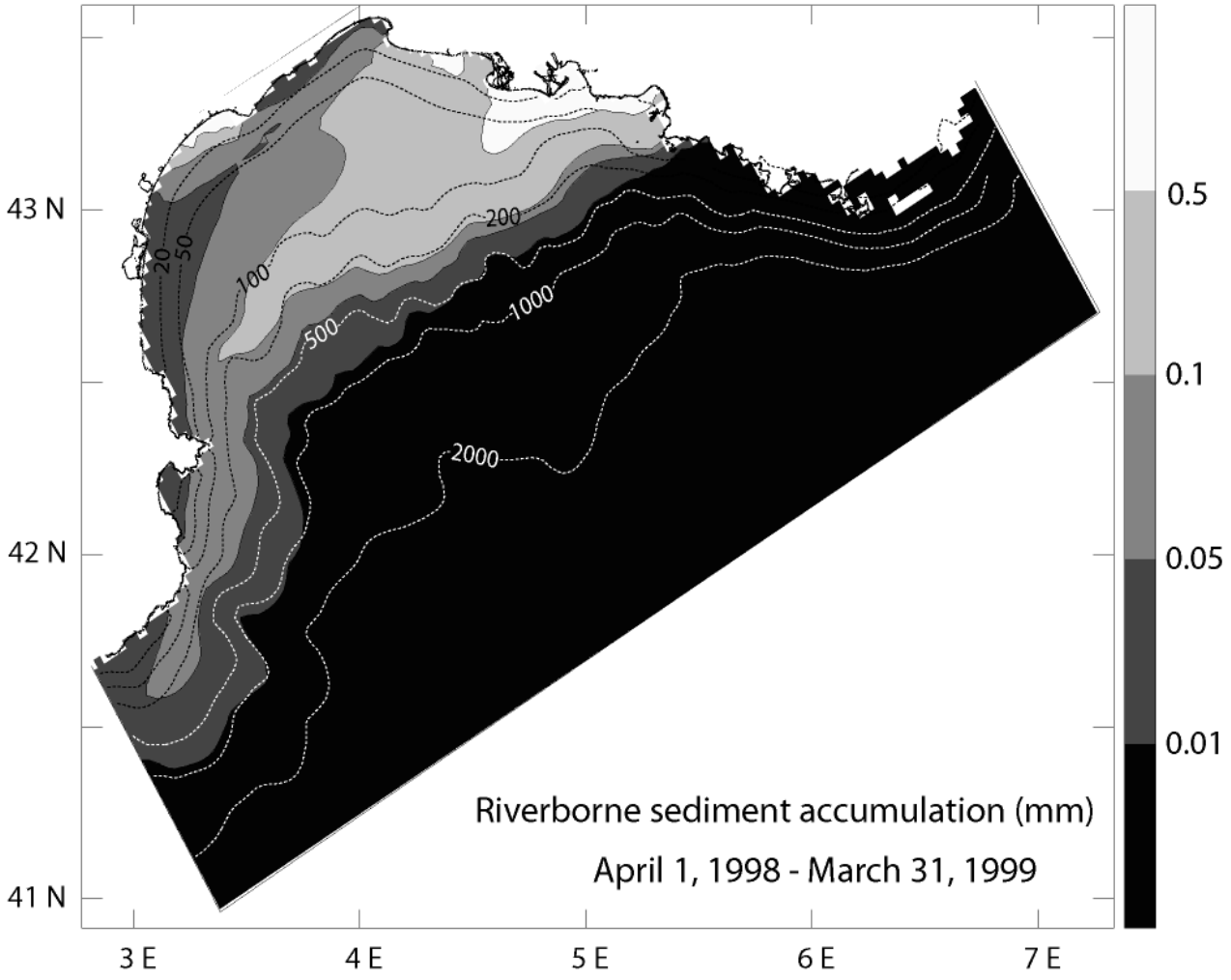

998 Ferre et al. Figure 4

999

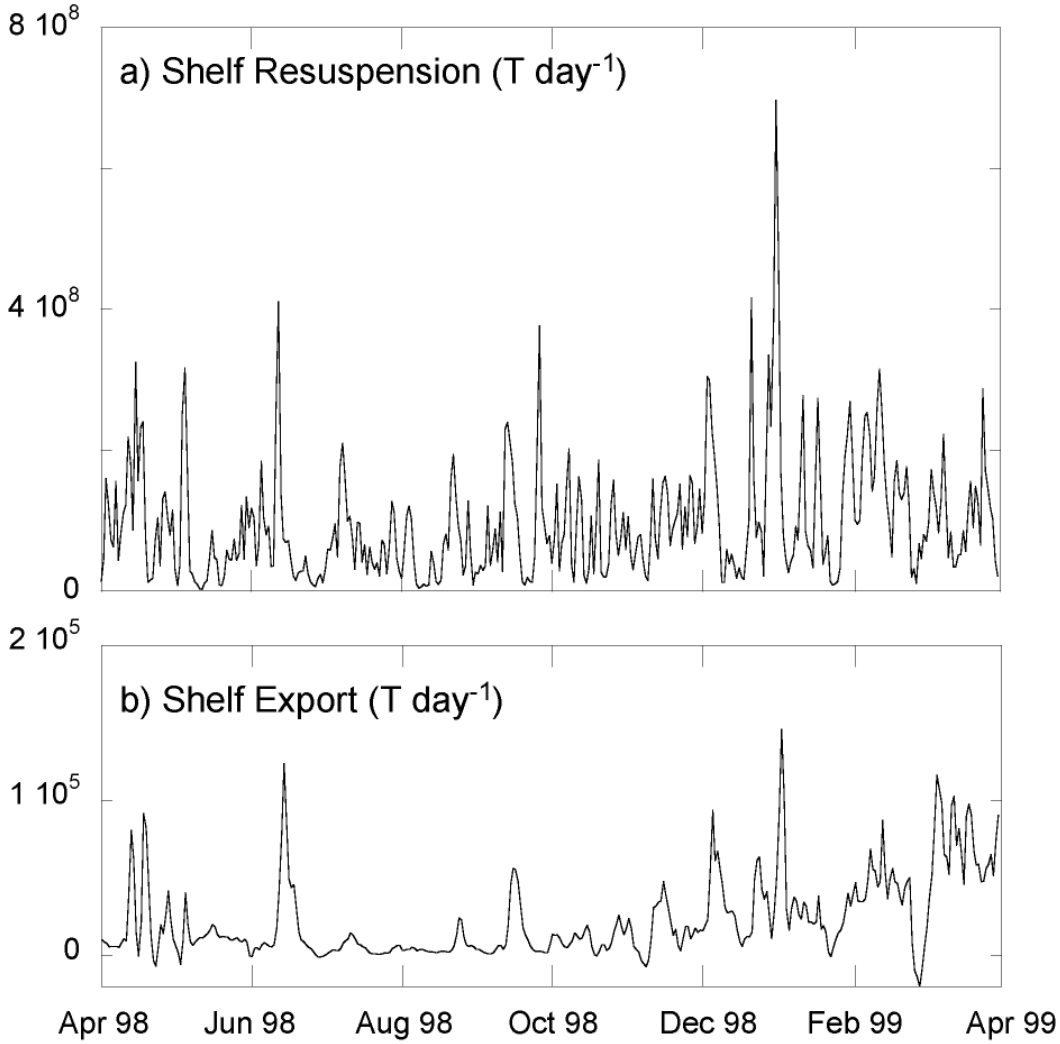

Ferre et al. Figure 5

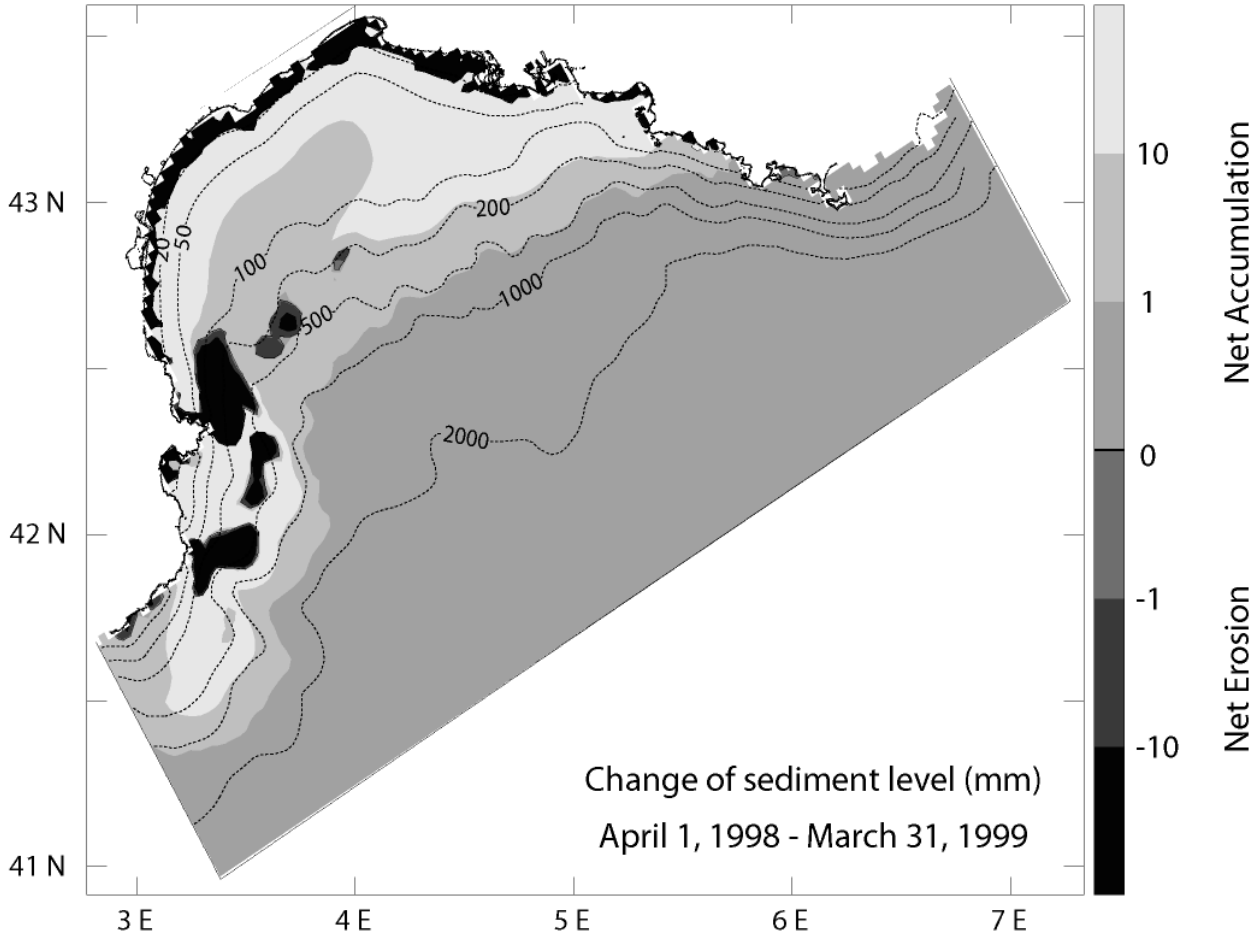

Ferre et al. Figure 6

1017

1018

1019

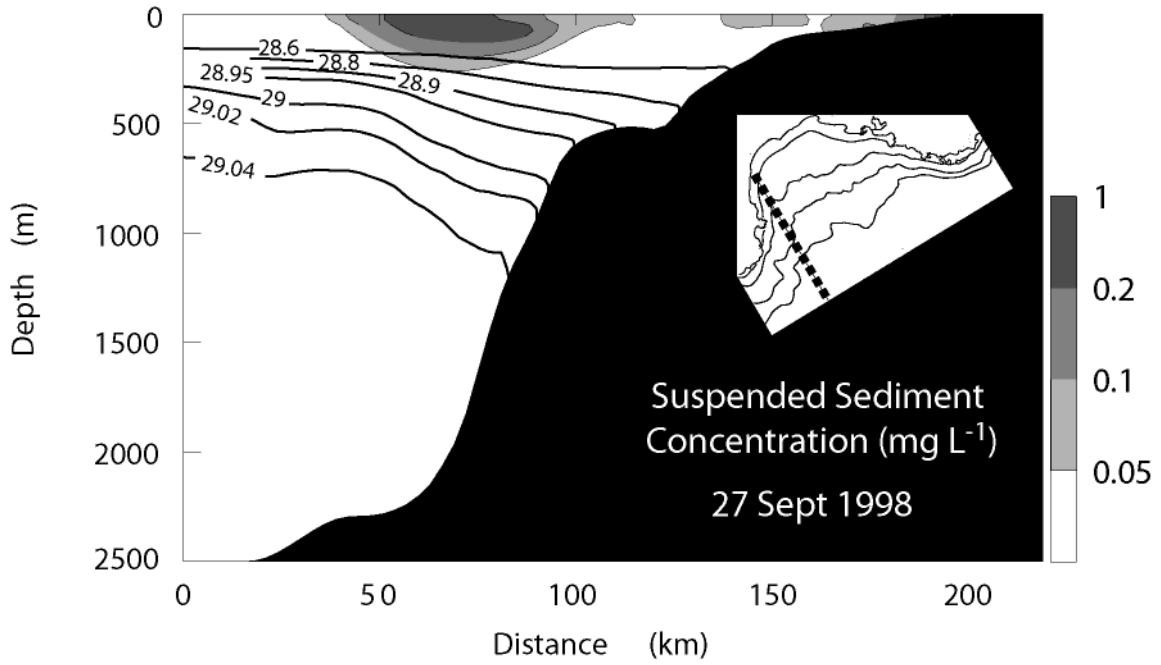

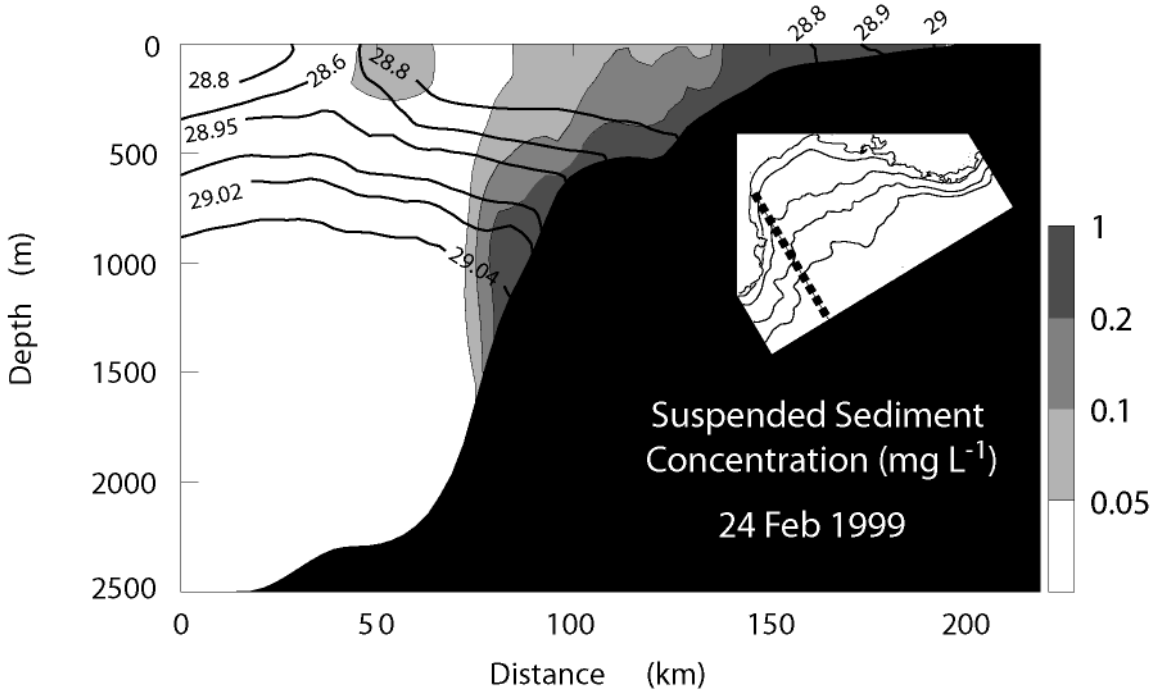

Ferre et al. Figure 7

1020

1021

1022

1023

1024

1025

1026

1027

1028

1029

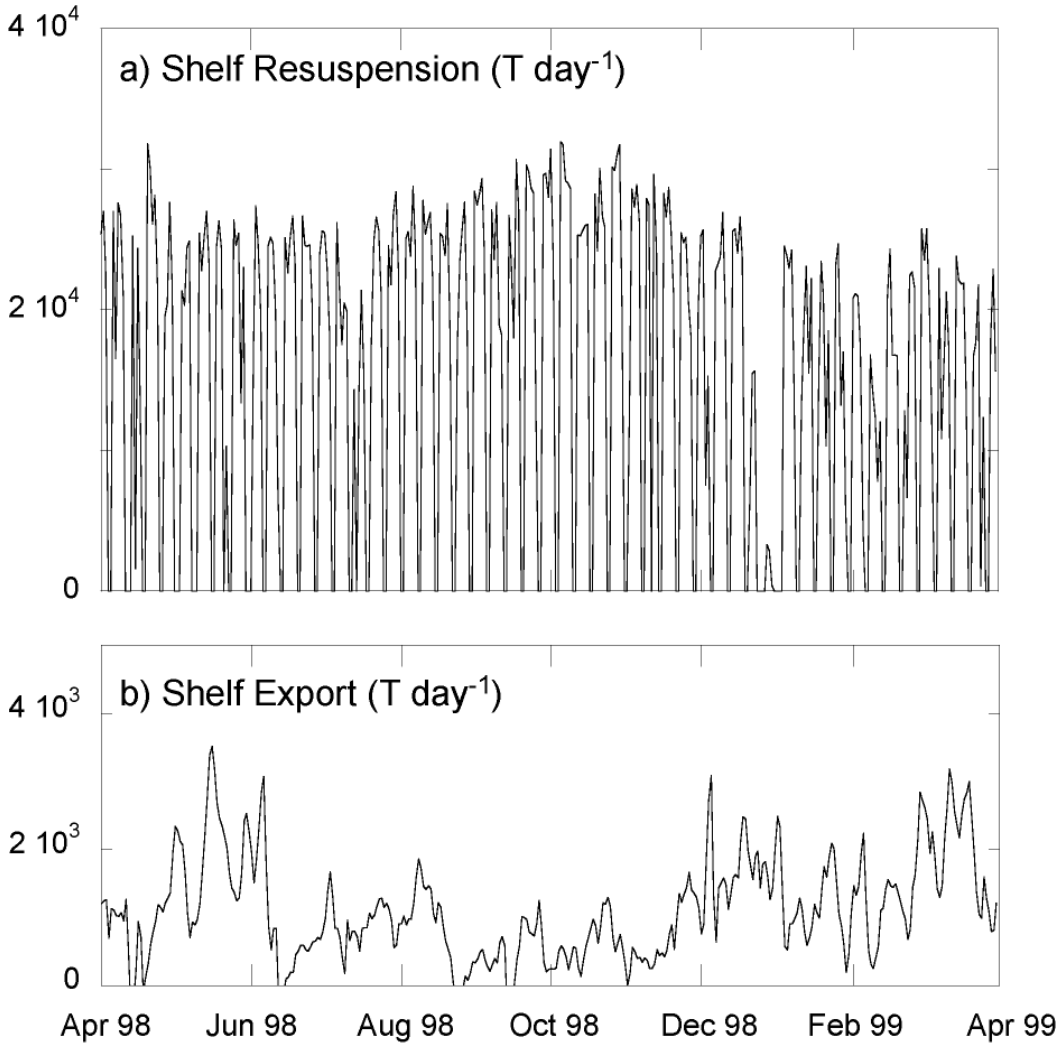

1030 Ferre et al. Figure 8

1031

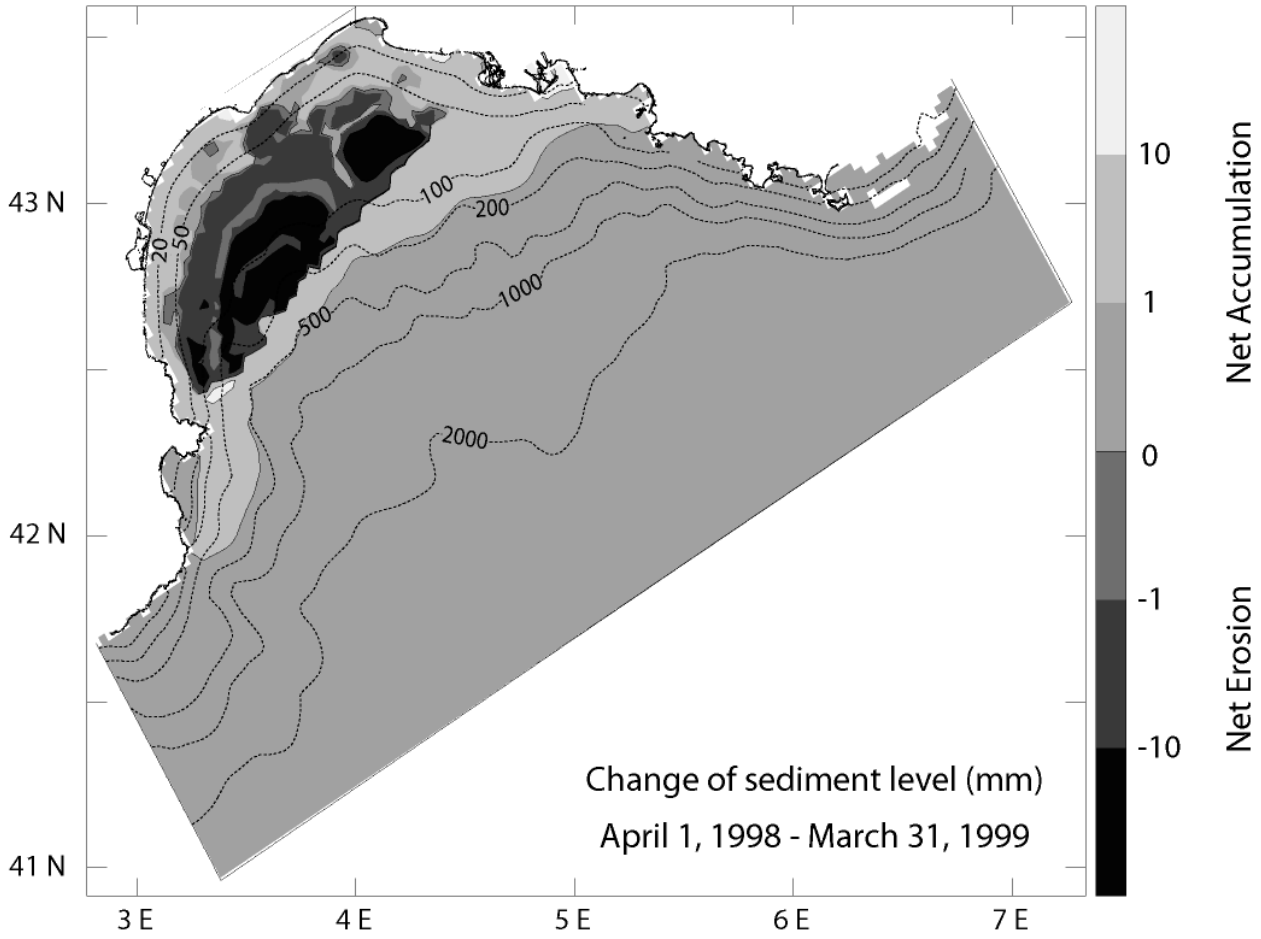

Ferre et al. Figure 9

1039

1040

1041

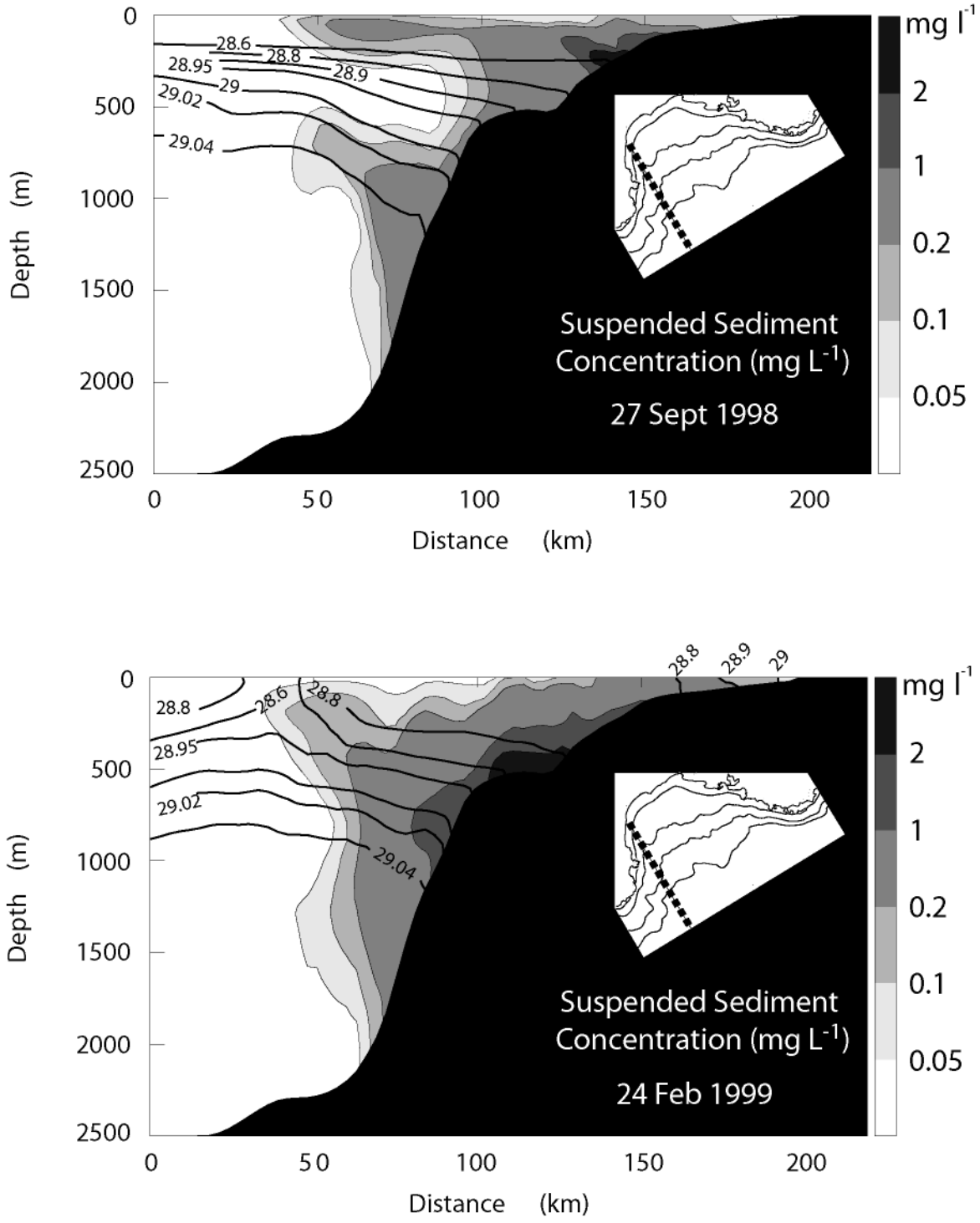

1042

Ferre et al. Figure 10

1043

1044

1045

1046

1047

1048

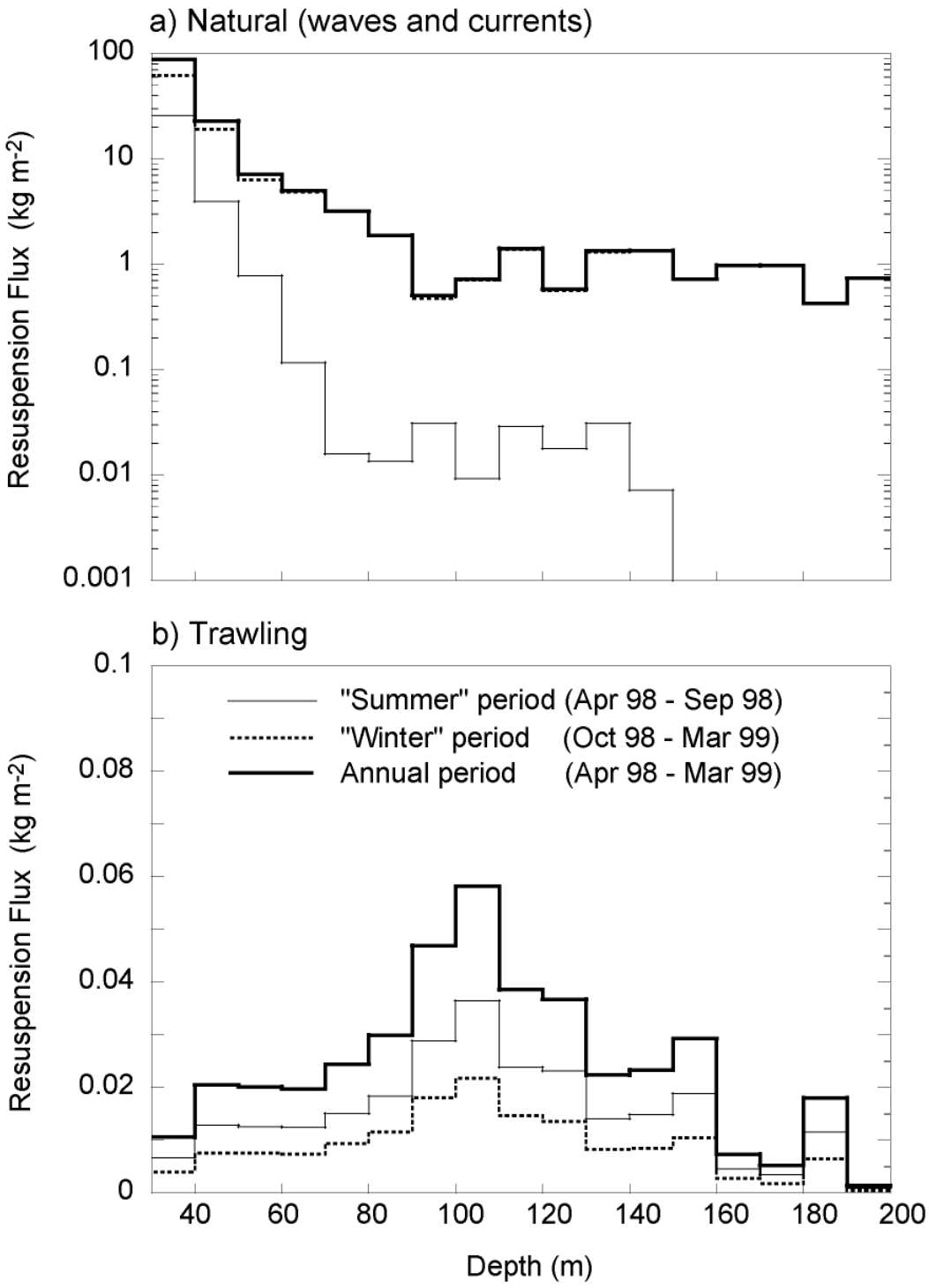

Ferre et al. Figure 11

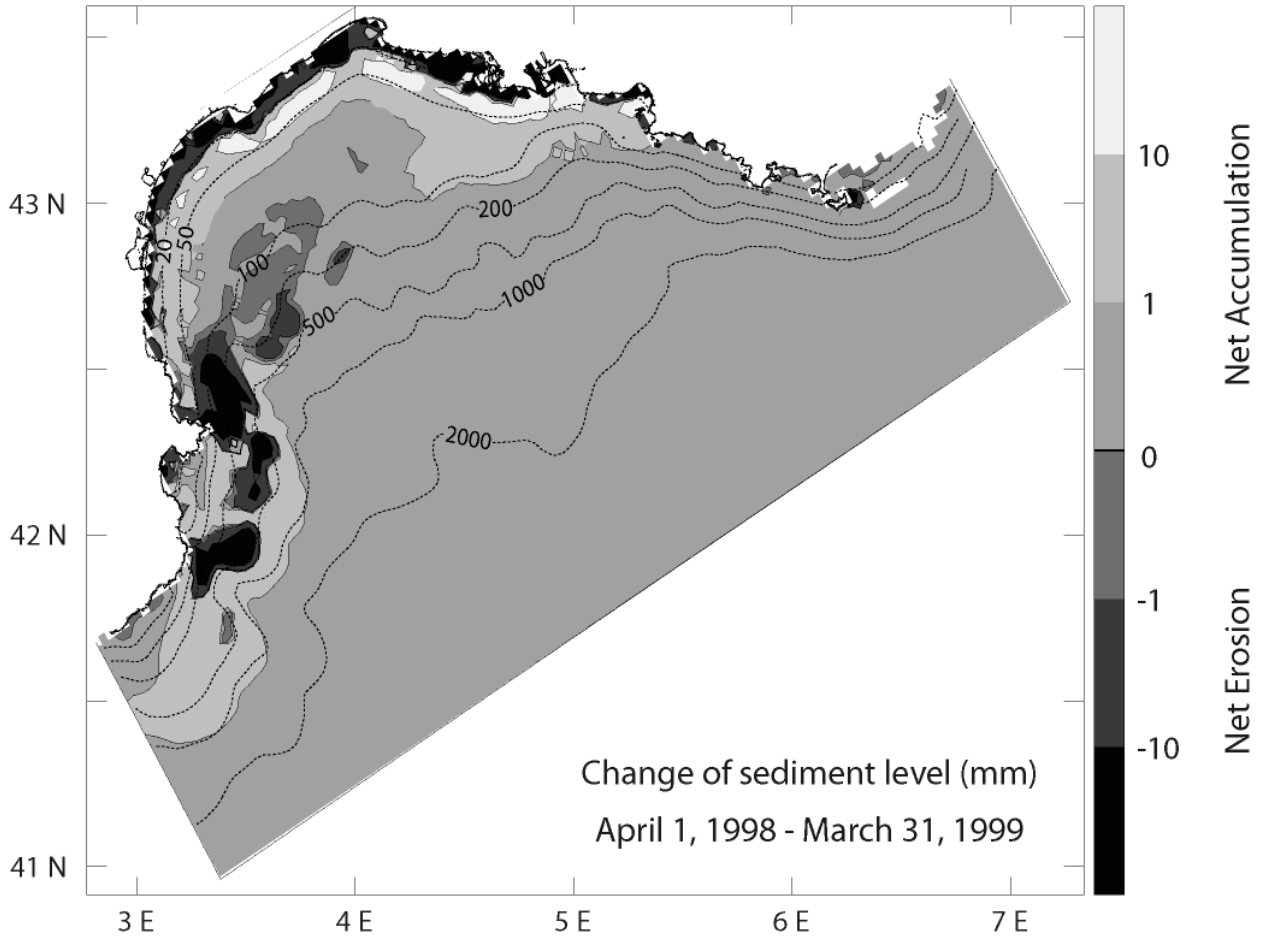

Ferre et al. Figure 12

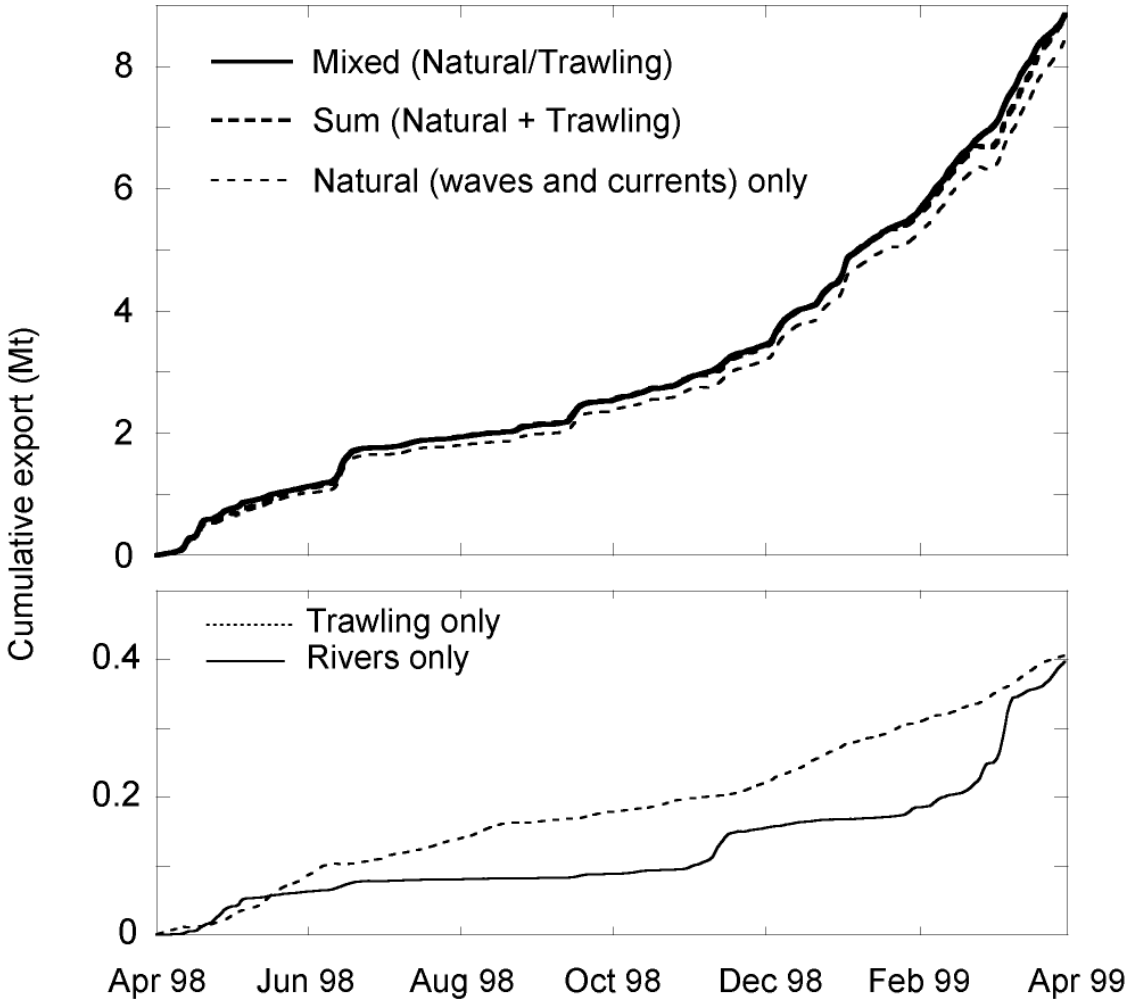

Ferre et al. Figure 13

1067 Table 1. Characteristics of particle grain size classes used in the sediment transport model

1068

Class	**1**	**2**	**3**	**4**	**5**	**6**	**7**	**8**	**9**
category	clay	Fine silt	Coarse silt	Very find sand	Fine sand	Median sand	Coarse sand	Aggregates	
D_{50} (μm)	2.43	8.39	31.6	92.4	179.21	317	1063	31.6	129.5
W_s (m s^{-1})	4.6×10^{-6}	5.5×10^{-5}	7.7×10^{-4}	6.6×10^{-3}	2.0×10^{-2}	4.1×10^{-2}	1.6×10^{-1}	1.1×10^{-4}	5.9×10^{-4}
ρ (kg m^{-3})	2650	2650	2650	2650	2650	2650	2650	1264	1097

1069

1070

Table 2. Annual sediment fluxes integrated between April 01, 1998 and March 31, 1999. Scenarios with Storms and /or Trawling resuspension include sediment input by rivers. Deposition rate for these scenarios excludes the deposited and exported sediment directly deriving from rivers. Once riverine sediment has been deposited on the shelf it is accounted in the resuspension, and subsequent deposition and export fluxes.

Scenario / **Sed Fluxes**	**Rivers**	**Storms**	**Trawling**	**Sum (Storms + Trawling)**	**Mixed (Storms and Trawling)**
River Discharge (10^6 T y^{-1})	3.6	3.6	3.6	3.6	3.6
Shelf Erosion (10^6 T y^{-1})	0	35264.6	5.6	35270.2	35209.4
Shelf Deposition (10^6 T y^{-1})	3.1	35255.4	5.2	35260.6	35200.1
Shelf (Erosion-Deposition) (10^6 T y^{-1})	-3.1	9.2	0.4	9.6	9.3
Shelf export (10^6 T y^{-1})	0.4	8.5	0.4	8.9	8.9